



## Article

<https://doi.org/10.1038/s43018-024-00810-4>

# A targetable type III immune response with increase of IL-17A expressing CD4<sup>+</sup> T cells is associated with immunotherapy-induced toxicity in melanoma

Received: 1 December 2023

Accepted: 18 July 2024

Published online: 29 August 2024

Check for updates

Florentia Dimitriou <sup>1,2</sup>✉, Phil F. Cheng <sup>1,2,3</sup>, Annalisa Saltari <sup>1,2</sup>,  
Katrín Schaper-Gerhardt <sup>4,5</sup>, Ramon Staeger <sup>1,2</sup>, Veronika Haunerdinger <sup>1,2</sup>,  
Federica Sella <sup>1,2</sup>, Aizhan Tastanova <sup>1,2</sup>, Christian Urban <sup>6</sup>, Susanne Dettwiler <sup>7</sup>,  
Daniela Mihic-Probst <sup>2,7</sup>, Christian M. Matter <sup>8</sup>, Olivier Michelin <sup>3</sup>,  
Ralf Gutzmer <sup>4</sup>, Georgina V. Long <sup>9,10,11</sup>, Burkhard Becher <sup>12</sup>,  
Mitchell P. Levesque <sup>1,2,13</sup> & Reinhard Dummer <sup>1,2,13</sup>✉

Immune checkpoint inhibitors are standard-of-care for the treatment of advanced melanoma, but their use is limited by immune-related adverse events. Proteomic analyses and multiplex cytokine and chemokine assays from serum at baseline and at the adverse event onset indicated aberrant T cell activity with differential expression of type I and III immune signatures. This was in line with the finding of an increase in the proportion of CD4<sup>+</sup> T cells with IL-17A expression at the adverse event onset in the peripheral blood using flow cytometry. Multiplex immunohistochemistry and spatial transcriptomics on immunotherapy-induced skin rash and colitis showed an increase in the proportion of CD4<sup>+</sup> T cells with IL-17A expression. Anti-IL-17A was administered in two patients with mild myocarditis, colitis and skin rash with resolution of the adverse events. This study highlights the potential role of type III CD4<sup>+</sup> T cells in adverse event development and provides proof-of-principle evidence for a clinical trial using anti-IL-17A for treating adverse events.

Immune checkpoint inhibitors (ICIs) block the immunosuppressive milieu that promotes tumorigenesis and tumor progression and are therefore established for the treatment of multiple malignancies, including melanoma<sup>1</sup>. This disturbance of the homeostatic mechanisms of immune tolerance may lead to various toxicities, referred to as immune-related adverse events (irAEs)<sup>2</sup>. Severe (grade  $\geq 3$ ) irAEs leading to systemic corticosteroid administration and hospitalization have been reported in 17% of patients treated with single-agent anti-PD1 (ref. 3); they occur more frequently when ICIs are combined<sup>4</sup>. Although these irAEs are generally manageable with the administration of systemic corticosteroids or other immunomodulatory agents<sup>5,6</sup>, they represent a significant source of morbidity and can be rarely associated

with long-term functional organ impairment<sup>7</sup> or even fatality<sup>8</sup>. Hence, treatment strategies to mitigate irAEs without compromising antitumor immunity are urgently needed.

A comprehensive mechanistic understanding of the development of irAEs is currently missing. Some of the main components involved in irAE occurrence include autoreactive and cross-reactive T cells and B cells against tumor-specific antigens<sup>9–11</sup>, complement-mediated inflammation<sup>12,13</sup> and expansion of pre-existing autoantibodies produced by B cells<sup>14,15</sup>. Ultimately, irAEs are linked to the mechanism of action of ICIs, which results in alterations of the systemic immunity; CTLA4 inhibition leads to increased priming and activation of antigen-specific T cells, whereas inhibition of PD1 signaling stimulates

A full list of affiliations appears at the end of the paper. ✉e-mail: florentia.dimitriou@usz.ch; Reinhard.Dummer@usz.ch

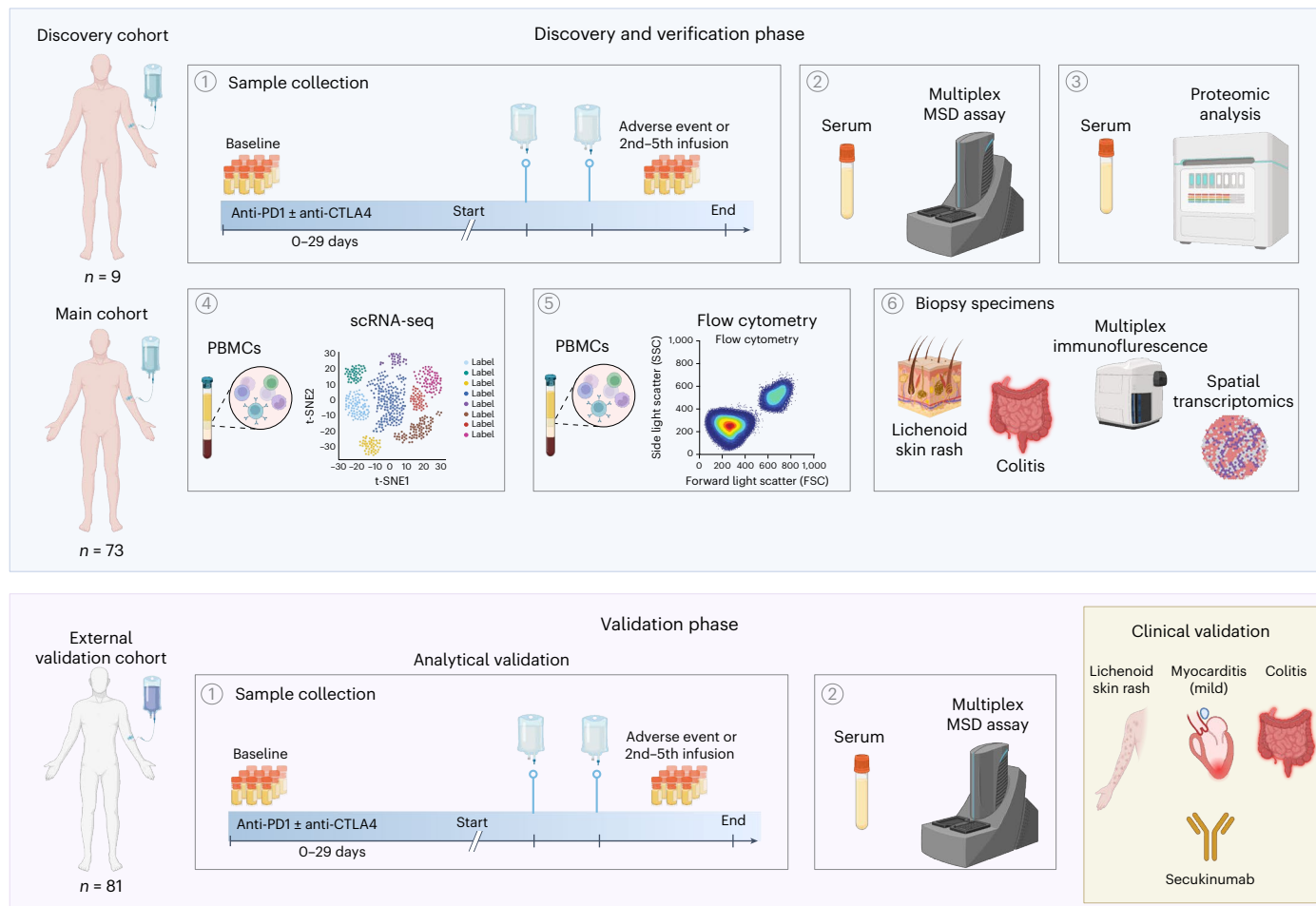


**Fig. 1 | Study design.** Overview of the patients included in the study and downstream analyses that were performed. Created with BioRender.com.

oligo-clonal expansion of T cells at the tumor site<sup>14</sup>. Activated T cells are primed towards a certain lineage, which is regulated by stimulating and inhibiting cytokines. To comprehensively describe this helper T cell ( $T_H$ ) plasticity, three types of responses that are based on the primary engaged target cells have been proposed: type I is triggered by intracellular pathogens with the production of IFN $\gamma$  and GM-CSF; type II supports the development of cellular immunity with the production of IL-4, IL-5 and IL-13; and type III is initiated at barrier sites, such as the skin, gut and other mucosal tissue<sup>16</sup>. Critical cytokines of the type III  $T_H$  cells include IL-17 and IL-22, which are expressed throughout the stromal and immune compartment, and their dysregulation has been implicated in various diseases of barrier tissues<sup>17–19</sup>. Type III cytokines, such as IL-6, have also been linked to the occurrence of irAEs in patients treated for melanoma<sup>20,21</sup>. These data, alongside the successful use of cytokine-blocking treatments in the management of corticosteroid-refractory irAEs<sup>22,23</sup>, raise the possibility of additional therapeutic strategies in addition to the standard use of corticosteroids. Based on these findings, we designed a translational study to comprehensively analyze the immune biology of irAEs and propose possible treatment strategies in addition to the standard administration of systemic corticosteroids.

## Results

### Increase of cytokines and chemokines in patients with severe irAEs

We systematically analyzed serum proteome and circulating chemokines and cytokines from peripheral blood collected at baseline (0–29 days before therapy initiation) and at the irAEs onset or at

the second to fifth infusion (in patients without any irAEs), in patients with advanced melanoma treated with anti-PD1-based ICIs, including single-agent anti-PD1 (pembrolizumab and nivolumab) or in combination with anti-CTLA4 (ipilimumab) in a discovery, verification and validation cohort (Fig. 1). As an initial approach to investigate the correlation of specific cytokines and chemokines with the onset of irAEs, we used a discovery cohort of nine patients with stage IV melanoma and severe (grade  $\geq 3$ ) irAEs during the treatment course of ipilimumab and nivolumab. This discovery cohort was used as an exploratory cohort to investigate the correlation of specific cytokines and chemokines with the onset of the irAEs. For this purpose, serum samples that were collected at the baseline served as controls to investigate the change of specific cytokines and chemokines in samples collected at the onset of the irAEs. Based on the results of this analysis, a study protocol was established for prospective sample collection in a main study cohort, in which patients with irAEs (cases) were compared to control patients without irAEs.

Serum samples were analyzed using a panel of 33 cytokines and chemokines with the U-PLEX Assay Platform (Meso Scale Diagnostics (MSD)). Patients were retrospectively selected according to the availability of serum samples at baseline and at the onset of an irAE from an initial cohort of 53 patients with similar treatment and irAE characteristics. Baseline characteristics are summarized in Supplementary Table 1. Seven patients (78%) had multiple, concurrent irAEs that included  $\geq 2$  systemic organs, and the most common irAEs included immune-related colitis (5 out of 9, 56%), ir-hepatitis (3 out of 9, 33%) and skin rash (3 out of 9, 33%). Initial analyses of the serum cytokines and chemokines at baseline using a multiplex chemokine/cytokine assay revealed that

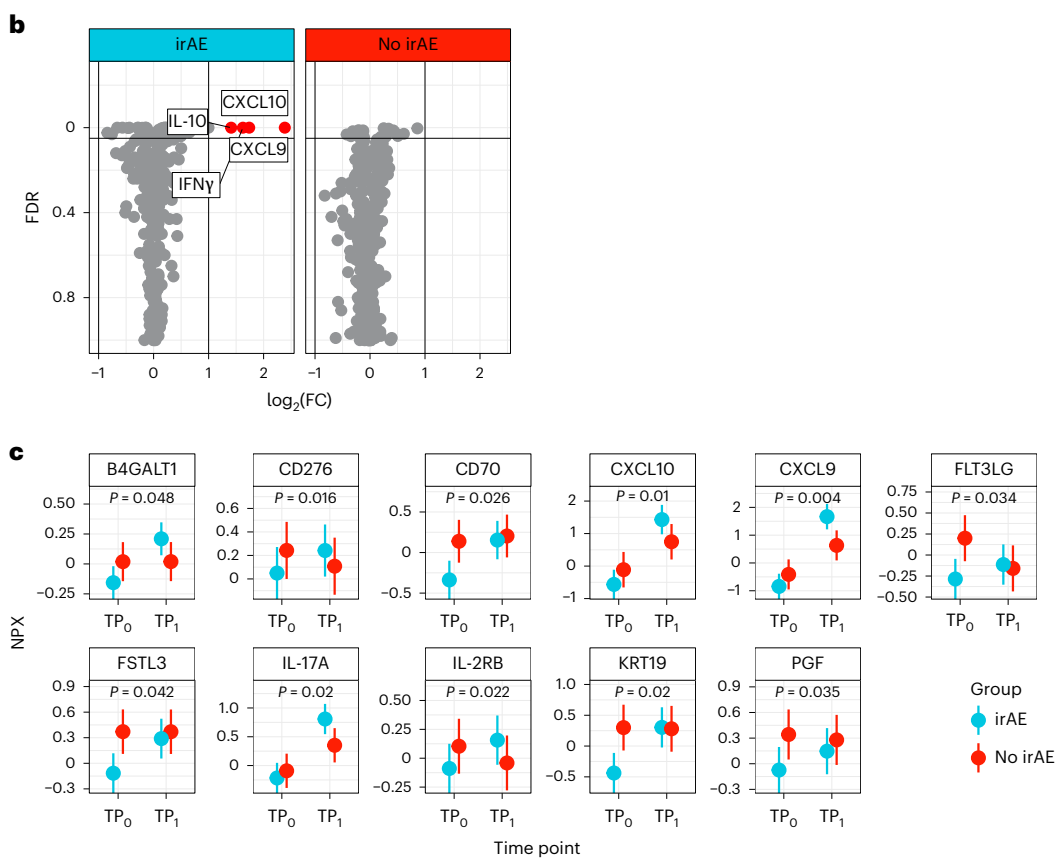
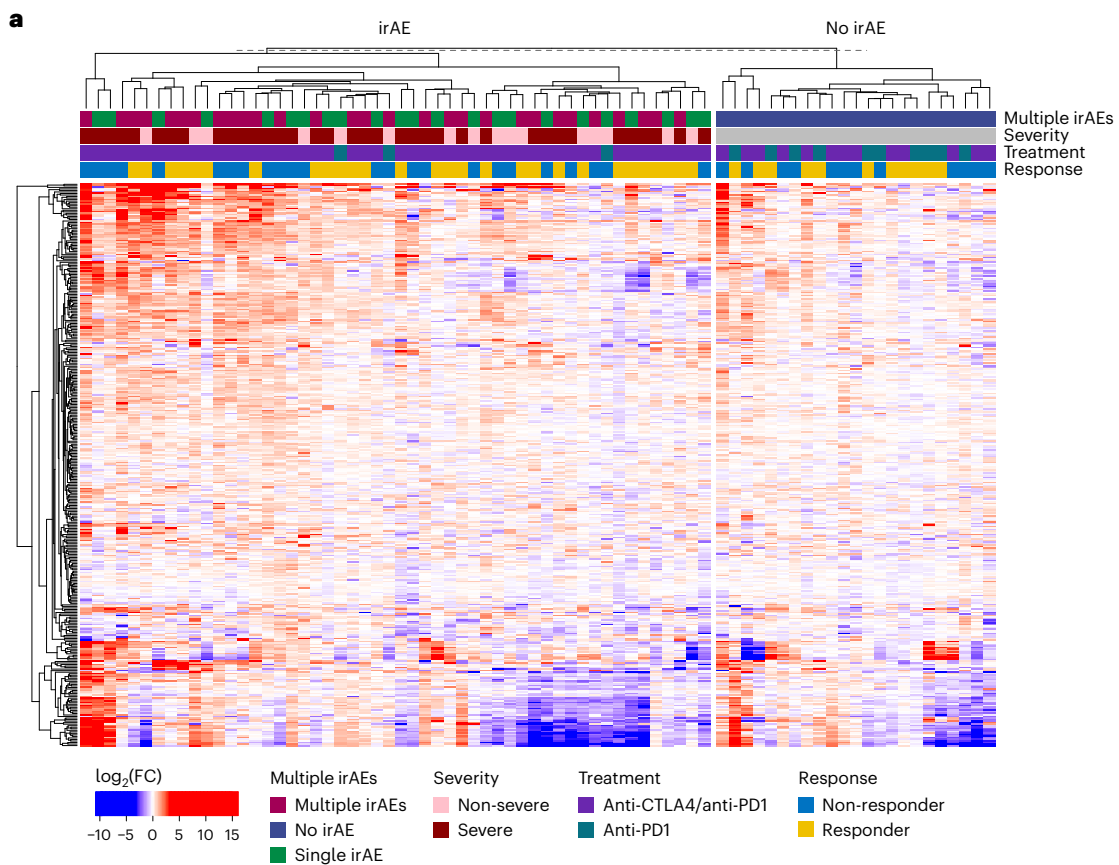


**Fig. 2 | Differential protein analysis by Olink in the main study cohort.**

**a**, Heatmap of  $\log_2(\text{FC})$  of the 384 serum proteins in  $n = 73$  patients with and without irAEs in the main study cohort. **b**, Volcano plot with the differential expressed proteins at baseline ( $TP_0$ ) and at irAE onset (in patients with irAEs) or at the second to fifth infusion (in patients without irAEs) ( $TP_1$ ) in the main study cohort ( $n = 73$  patients). Significant difference was determined by a two-sided

Wilcoxon rank sum test, and  $P$  values were adjusted by the Benjamini–Hochberg method. FDR, false discovery rate; FC, fold change. **c**, Linear mixed-effects regression analysis of the 11 significant proteins for the two time points ( $TP_0$  and  $TP_1$ ) in  $n = 73$  patients with and without irAEs. Data are represented by the estimated marginal means with 95% confidence intervals. The y axis represents the Olink assay value (NPX).  $P$  values are adjusted using the Tukey method.

most cytokines and chemokines were expressed at low levels, which increased at irAE onset (Extended Data Fig. 1a,b). In a Wilcoxon rank sum test analysis for the significant cytokines and chemokines, IL-17A showed the highest  $\log_2(\text{fold change})$  from baseline to irAE onset (3.81,  $P < 0.01$ , respectively); of note, the IL-17A elevation at irAE onset was overall consistent. Further cytokines and chemokines included IFN $\gamma$  (3.77,  $P < 0.01$ ), CXCL9 (3.02,  $P < 0.01$ ), CXCL11 (2.3,  $P < 0.01$ ), IL-10 (2.28,  $P < 0.01$ ), IL-21 (2.06,  $P < 0.01$ ), CXCL10 (1.91,  $P < 0.01$ ) and TNF (1.79,  $P < 0.01$ ).

**Proteomic analyses of serum proteins at the onset of irAEs**

A proteomic analysis based on the proximity extension assay technology and the use of Olink Explore 384 Inflammation panel on serum samples prospectively collected at baseline and the onset of irAEs or at the second to fifth infusion (in patients without irAEs) was implemented in a main study cohort of 73 patients. Patient characteristics are described in Supplementary Table 1. Overall, 49 out of 73 patients (67%) developed irAEs, 29 out of 73 (40%) had multiple ( $\geq 2$ ) concurrent irAEs and 34 out of 73 (47%) had severe (grade  $\geq 3$ ) irAEs. The median time to irAEs onset was 27 days (range, 1–91 days). The overall response rate was 49%.

Patients with irAEs had higher  $\log_2(\text{fold change})$  in several proteins of this panel than those without any irAEs (Fig. 2a). For the differential protein analysis between the two time points, namely  $TP_0$  (baseline) and  $TP_1$  (irAEs onset or second to fifth infusion), we considered a fold change of two as a relevant change, which corresponds to a  $\log_2(\text{fold change})$  of  $>1$ , with an adjusted  $P$  value of  $\leq 0.05$ . Using the Wilcoxon rank sum test, four proteins showed a significant differential expression from  $TP_0$  to  $TP_1$  in patients with irAEs; these included CXCL9, CXCL10, IFN $\gamma$  and IL-10 (Fig. 2b). None of these proteins showed any significant change in patients without irAEs. The same test was performed for the differential protein analysis in patients with multiple ( $\geq 2$ ) irAEs compared to those with single irAEs (Extended Data Fig. 2a) as well as those with severe (grade  $\geq 3$ ) irAEs compared to those with non-severe (grade 1–2) irAEs (Extended Data Fig. 2b). Notably, the differential expression of the significant proteins in patients with multiple ( $\geq 2$ ) irAEs and those with severe (grade  $\geq 3$ ) irAEs was similar and included eight overlapping proteins: CXCL9, CXCL10, IL-10, IFN $\gamma$ , GZMA, FABP1, TNF and SULT2A1. To further characterize the significant proteins that were differentially expressed between  $TP_0$  and  $TP_1$ , and to analyze these results in one statistical model, we identified proteins that significantly changed over time and between the two patient groups, namely those with and without irAEs, using a linear mixed-effect model for the time and the occurrence of the irAEs. Other covariates, including age, sex and treatment type, were integrated into the model, and each patient was added as a random effect. Using this statistical model, 11 proteins showed the highest differential expression from baseline to the irAE onset in patients with irAEs (all  $P < 0.01$ ; Fig. 2c). These included (1) CXCL9, which has chemotactic functions and regulates

the immune cell migration, differentiation and activation<sup>24</sup>; (2) IL-17A, a pro-inflammatory cytokine produced by activated T cells<sup>25</sup>; (3) IL-15, a pleiotropic inflammatory cytokine that regulates the homeostasis of both innate and adaptive immune cells<sup>26</sup>; (4) keratin 19 (KRT19), a protein-coding gene that encodes the protein CYFRA21.1, a member of the keratin family<sup>27</sup>; (5) CD276, a type I transmembrane protein that suppresses T cell activation and proliferation in non-malignant tissues<sup>28</sup>; (6) IL2RB, which is involved in T cell-mediated immune responses and increases proliferation of CD8 $+$  effector T cells<sup>29</sup>; (7) CD70, which has an important role in the regulation of the immune system activation<sup>30</sup>; (8) follistatin-related protein 3 (FSTL3), a secreted glycoprotein of the follistatin-module-protein family<sup>31</sup>; (9) Fms-related tyrosine kinase 3 ligand (FLT3LG), which stimulates the proliferation and differentiation of various blood cell progenitors, including the growth of dendritic cells<sup>32</sup>; (10) beta-1,4-galactosyltransferase 1 (B4GALT1), which is overexpressed in pathological processes, including inflammation and proliferation of cancer cells<sup>33</sup>; and (11) placental growth factor, a member of the vascular endothelial growth factor (VEGF) sub-family, a key molecule in angiogenesis and vasculogenesis<sup>34</sup>. Of note, some of these proteins also increased over time in patients without irAEs, but these changes were not significant in the linear mixed-effect model (Fig. 2c). None of these proteins was predictive for the occurrence of irAEs at baseline.

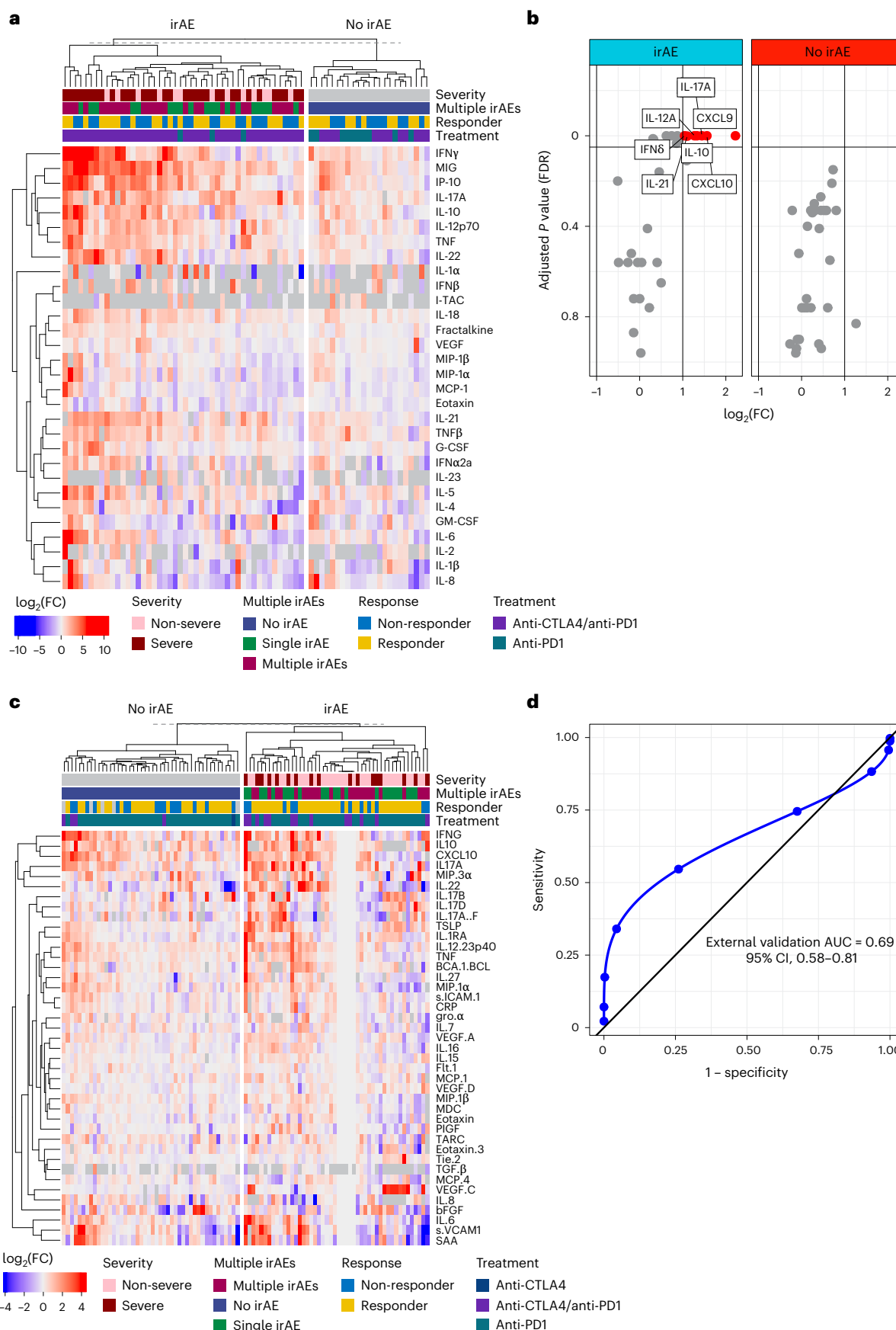
Next, the differential protein expression was analyzed according to the treatment response; using the Wilcoxon rank sum test, responders and non-responders showed a significant increase in specific proteins from  $TP_0$  to  $TP_1$ , which included CXCL9, IL-10 and IFN $\gamma$  in responders, and CXCL9 and CXCL10 in non-responders (false discovery rate-adjusted  $P \leq 0.05$  and  $\log_2(\text{fold change}) > 1$ ; Extended Data Fig. 2c). To further analyze these results in one statistical model, a linear mixed-effect model for the time, treatment response and occurrence of the irAEs was used. This statistical model was adjusted for age and sex. None of the 11 proteins that showed the highest expression in patients with irAEs was significant for the type of treatment response (Extended Data Fig. 2d). Overall, this analysis shows that specific proteins are significantly upregulated at the time of the irAE onset in patients with irAEs.

**Increase of type I and III cytokines and chemokines at the onset of irAEs**

A multiplex chemokine/cytokine assay with the selected panel of 33 cytokines and chemokines described above (MSD) was applied to further validate these results in the main study cohort. Of note, the MSD technology provides a multiplex assay of high sensitivity and broad dynamic range for investigating cytokines and chemokines using electrochemiluminescence, which allows for technical validation of the results with high accuracy<sup>35</sup>. Similar to the proteomic analysis, patients with irAEs showed higher  $\log_2(\text{fold change})$  in several cytokines and chemokines than those without any irAEs (Fig. 3a), as did patients

**Fig. 3 | Multiplex MSD assay with a selected panel of 33 cytokines and chemokines in the main study cohort.** **a**, Heatmap of  $\log_2(\text{fold change})$  of the serum cytokines and chemokines per patient in the multiplex MSD assay at the baseline ( $TP_0$ ) and at the irAE onset (in patients with irAEs) or at the second to fifth infusion (in patients without irAEs) ( $TP_1$ ) in the main study cohort ( $n = 73$  patients). **b**, Volcano plot with the differential expressed proteins at  $TP_0$  and  $TP_1$  in patients with and without irAEs in the multiplex MSD assay in the main study cohort ( $n = 73$  patients). Significant difference was determined by a two-sided

Wilcoxon rank sum test, and  $P$  values were adjusted by the Benjamini–Hochberg method. **c**, Heatmap of  $\log_2(\text{fold change})$  of the serum cytokines and chemokines per patient in the multiplex MSD assay at  $TP_0$  and  $TP_1$  in the external validation cohort ( $n = 81$  patients). **d**, Receiver operating characteristic curve analysis of the five cytokine and chemokine panels that were significantly differentially expressed in the main study cohort ( $n = 73$  patients) for the association with the irAE onset in the external validation cohort ( $n = 81$  patients). AUC, area under the curve.



with multiple ( $\geq 2$ ) irAEs (Extended Data Fig. 3). Using the Wilcoxon rank sum test, seven cytokines and chemokines showed the highest  $\log_2(\text{fold change})$  from  $\text{TP}_0$  to  $\text{TP}_1$  in patients with irAEs, including CXCL9, CXCL10, IL-17A, IL-12A, IL-10, IL-21 and IFNy (false discovery rate-adjusted  $P \leq 0.05$  and  $\log_2(\text{fold change}) > 1$ ; Fig. 3b).

The analytical validation of these results was performed in an independent external validation cohort of  $n = 81$  patients using a similar multiplex cytokine–chemokine assay (MSD). The baseline characteristics of this cohort are summarized in Supplementary Table 1. In line with the previous observations, most cytokines and chemokines increased from  $\text{TP}_0$  to  $\text{TP}_1$  (Fig. 3c). Of note, CXCL9 and IL-21 were not included in the multiplex cytokine–chemokine assay of the external validation cohort. To analyze the performance of the five (out of seven) cytokines and chemokines that showed the highest  $\log_2(\text{fold change})$  in the verification phase of the study, namely CXCL10, IL-17A, IL-10, IL-12A and IFNy, we performed a receiver operating characteristics curve analysis and found an area under the curve of 0.69 (95% CI, 0.58–0.81) (Fig. 3d)<sup>36</sup>. Overall, these results allow for a reliable association of signaling activities at the onset of irAEs and further identification of possible therapeutic biomarkers.

### The cellular source of significant cytokines and chemokines

Single-cell RNA sequencing (scRNA-seq) analysis of peripheral blood mononuclear cells (PBMCs) collected at  $\text{TP}_0$  and  $\text{TP}_1$  was performed to identify the cellular source of the cytokines and chemokines involved in these conditions. Taking into consideration the non-specific changes in the cytokine and chemokine profiles in responders and non-responders, PBMCs from patients with similar responses to ICIs were selected to eliminate any potential bias in the interpretation of the results. As such, PBMCs from six patients treated with ipilimumab and nivolumab with a partial response to the systemic treatment as the best overall response were analyzed using scRNA-seq. Three patients had grade  $\geq 3$  irAEs and three patients did not develop any irAEs during the treatment course. The single-cell data were analyzed using the Seurat R package, and cells were typed with SingleR using the Monaco Immune Data reference (GSE107011). Dimension reduction by principal component analysis (PCA), clustering by the Leiden algorithm and projection into 2D space by uniform manifold approximation and projection (UMAP) uncovered 24 distinct subpopulations from 117,702 cells. These cells were then evaluated, and eight major mononuclear lineages were encompassed, including B cells, CD4<sup>+</sup> and CD8<sup>+</sup> T cells, unspecified T cells, natural killer cells, monocytes, dendritic cells and progenitor cells (Fig. 4a). Dot plot analysis for the significantly differentially expressed cytokines and chemokines of the multiplex MSD assay in the main immune cell types showed an increased average expression of the type I cytokines and chemokines from  $\text{TP}_0$  to  $\text{TP}_1$  in patients with irAEs (Fig. 4b). The cellular source of the eight significant cytokines and chemokines that showed the highest  $\log_2(\text{fold change})$  from the baseline to the irAE onset was then visualized using UMAP and cell typing (Fig. 4c–n). In brief, CXCL9 and CXCL10 signals showed significant changes from  $\text{TP}_0$  to  $\text{TP}_1$  in patients with irAEs in monocytes and natural

killer cells, whereas IFNy was significantly expressed by CD4<sup>+</sup>, CD8<sup>+</sup> and natural killer cells from  $\text{TP}_0$  to  $\text{TP}_1$  in both patient groups. For IL-17A, no expression was detected.

Each subpopulation was then analyzed at  $\text{TP}_0$  and  $\text{TP}_1$ . The UMAP for each of these conditions showed that the transcriptomic profile of the immune cells altered from  $\text{TP}_0$  to  $\text{TP}_1$  in patients with irAEs (Extended Data Fig. 4). Next, we specifically looked for the T cell subtypes, which were visualized using UMAP (Fig. 5a). Differential gene expression analysis for the T cell subsets revealed a significant increase in STAT2 in all T cell subtypes in patients with irAEs and most T cell subtypes in patients without irAEs (Fig. 5b,c). By contrast, STAT3 was significantly increased in T<sub>H</sub>17 cells in patients with irAEs ( $P < 0.05$ ) (Fig. 5b,d). Of note, STAT3 was significantly increased in terminal effector CD8<sup>+</sup> T cells in patients without irAEs, which, alongside the existing literature involving the IL-10–IL-21–STAT3 pathway in the development of memory CD8<sup>+</sup> T cells<sup>37</sup>, might imply a higher activation of this pathway in patients without irAEs that respond to the ICI treatment. This finding should be investigated more rigorously in future studies.

### Increase of CD4<sup>+</sup> T cells with IL-17A expression at the irAEs onset

Cytokine signaling activity at a single-cell mRNA expression level in peripheral blood has several limitations. To limit the impact on the interpretation of previous results from scRNA-seq data, we additionally performed immunoprofiling of the T cells that are able to produce IL-17A<sup>38,39</sup> using flow cytometry in the PBMCs collected at  $\text{TP}_0$  and  $\text{TP}_1$  from the six patients of the above-mentioned cohort. The purpose of this analysis was to reliably delineate the cellular source of the IL-17A production at the irAE onset. We reasoned that dysregulation of the IL-17A-producing cells contributes to the onset of irAEs and that their immune signature can be used as therapeutic targets in these patients.

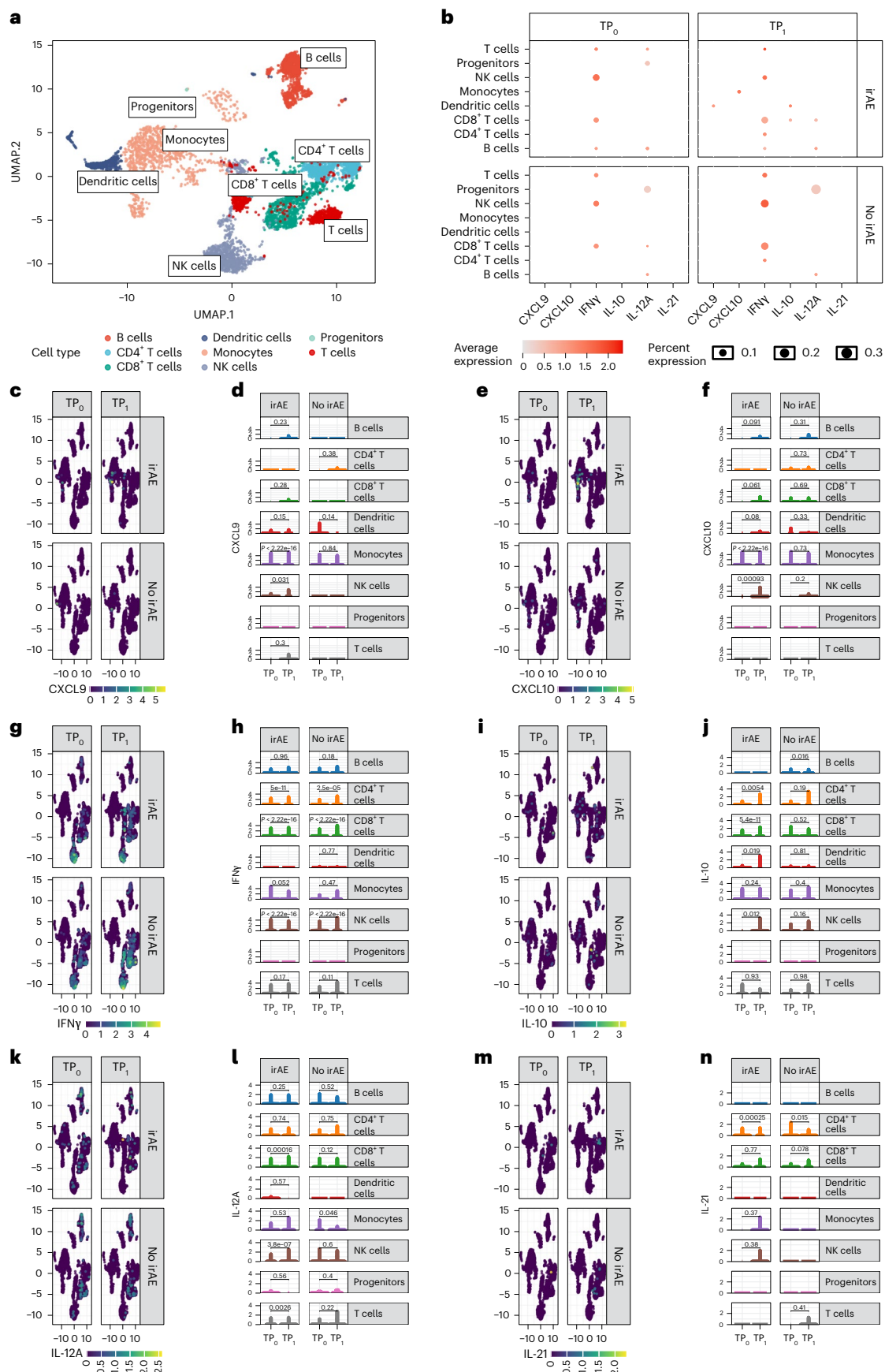
The collected PBMCs from patients with and without irAEs from  $\text{TP}_0$  and  $\text{TP}_1$  were stimulated for intracellular cytokine staining. For the cell type identification, antibodies targeting CD4<sup>+</sup> and CD8<sup>+</sup> T cells, B cells and γδ T cells were included (Extended Data Fig. 5 and Extended Data Fig. 6a). In the flow cytometry analysis, IL-17A production was only detectable in CD4<sup>+</sup> T cells (Extended Data Fig. 6b). The proportional analysis of the IL-17A-producing CD4<sup>+</sup> T cells for the two time points revealed a significant increase between patients with and without irAEs at  $\text{TP}_1$  ( $P = 0.05$ ), which was not present at  $\text{TP}_0$  ( $P = 0.2$ ) (Extended Data Fig. 6c). These results demonstrate that CD4<sup>+</sup> T cells are able to produce IL-17A at the irAE onset in patients with irAEs, thus underlining their substantial role in the occurrence of irAEs.

### T<sub>H</sub>17-mediated inflammation in colitis and skin rash samples

We next reasoned that the increase of the IL-17A-producing cells in the peripheral blood reflected changes at the site of occurrence of the irAEs. To address this hypothesis, multiplex immunofluorescence analysis of immune-related colitis and lichenoid skin rash samples of the six patients with available PBMCs that were included in the scRNA-seq analysis was performed, aiming to further elucidate the immune cells

**Fig. 4 | scRNA-seq analysis from PBMC samples at the baseline and at irAEs onset from three patients with irAEs and at the baseline and second to fifth infusion in three patients without any irAEs and response to immunotherapy.** **a**, UMAP plot, with overview of the main immune cell types for the above-mentioned conditions ( $n = 6$  patients). A total of 118,734 PBMCs were sequenced. NK, natural killer. **b**, Dot plot with the average expression of the significantly differentially expressed cytokines and chemokines from the multiplex MSD assay in the main immune cell types in the scRNA-seq analysis at the two time points ( $\text{TP}_0$  and  $\text{TP}_1$ ) for the six patients. The size of the dot represents the percentage of cells that show expression and the color of the dot represents the average expression. **c,d**, UMAP for CXCL9 for  $\text{TP}_0$  and  $\text{TP}_1$  in patients with and without irAEs ( $n = 6$ ) (**c**) and violin plot for the CXCL9 signal in main cell types for  $\text{TP}_0$  and  $\text{TP}_1$  in patients with and without irAEs ( $n = 6$ ) (**d**). **e,f**, UMAP for CXCL10 for  $\text{TP}_0$  and  $\text{TP}_1$  in patients with and without irAEs ( $n = 6$ ) (**e**) and violin plot for the CXCL10 signal in main cell types for  $\text{TP}_0$  and  $\text{TP}_1$  in patients with and without irAEs ( $n = 6$ ) (**f**). **g,h**, UMAP for IFNy for  $\text{TP}_0$  and  $\text{TP}_1$  in patients with and without irAEs ( $n = 6$ ) (**g**) and violin plot for the IFNy signal in main cell types for  $\text{TP}_0$  and  $\text{TP}_1$  in patients with and without irAEs ( $n = 6$ ) (**h**). **i,j**, UMAP for IL-10 for  $\text{TP}_0$  and  $\text{TP}_1$  in patients with and without irAEs ( $n = 6$ ) (**i**) and violin plot for the IL-10 signal in main cell types for  $\text{TP}_0$  and  $\text{TP}_1$  in patients with and without irAEs ( $n = 6$ ) (**j**). **k,l**, UMAP for IL-12A for  $\text{TP}_0$  and  $\text{TP}_1$  in patients with and without irAEs ( $n = 6$ ) (**k**) and violin plot for the IL-12A signal in main cell types for  $\text{TP}_0$  and  $\text{TP}_1$  in patients with and without irAEs ( $n = 6$ ) (**l**). **m,n**, UMAP for IL-21 for  $\text{TP}_0$  and  $\text{TP}_1$  in patients with and without irAEs ( $n = 6$ ) (**m**) and violin plot for the IL-21 signal in main cell types for  $\text{TP}_0$  and  $\text{TP}_1$  in patients with and without irAEs ( $n = 6$ ) (**n**).

**e,f**, UMAP for CXCL10 for  $\text{TP}_0$  and  $\text{TP}_1$  in patients with and without irAEs ( $n = 6$ ) (**e**) and violin plot for the CXCL10 signal in main cell types for  $\text{TP}_0$  and  $\text{TP}_1$  in patients with and without irAEs ( $n = 6$ ) (**f**). **g,h**, UMAP for IFNy for  $\text{TP}_0$  and  $\text{TP}_1$  in patients with and without irAEs ( $n = 6$ ) (**g**) and violin plot for the IFNy signal in main cell types for  $\text{TP}_0$  and  $\text{TP}_1$  in patients with and without irAEs ( $n = 6$ ) (**h**). **i,j**, UMAP for IL-10 for  $\text{TP}_0$  and  $\text{TP}_1$  in patients with and without irAEs ( $n = 6$ ) (**i**) and violin plot for the IL-10 signal in main cell types for  $\text{TP}_0$  and  $\text{TP}_1$  in patients with and without irAEs ( $n = 6$ ) (**j**). **k,l**, UMAP for IL-12A for  $\text{TP}_0$  and  $\text{TP}_1$  in patients with and without irAEs ( $n = 6$ ) (**k**) and violin plot for the IL-12A signal in main cell types for  $\text{TP}_0$  and  $\text{TP}_1$  in patients with and without irAEs ( $n = 6$ ) (**l**). **m,n**, UMAP for IL-21 for  $\text{TP}_0$  and  $\text{TP}_1$  in patients with and without irAEs ( $n = 6$ ) (**m**) and violin plot for the IL-21 signal in main cell types for  $\text{TP}_0$  and  $\text{TP}_1$  in patients with and without irAEs ( $n = 6$ ) (**n**).



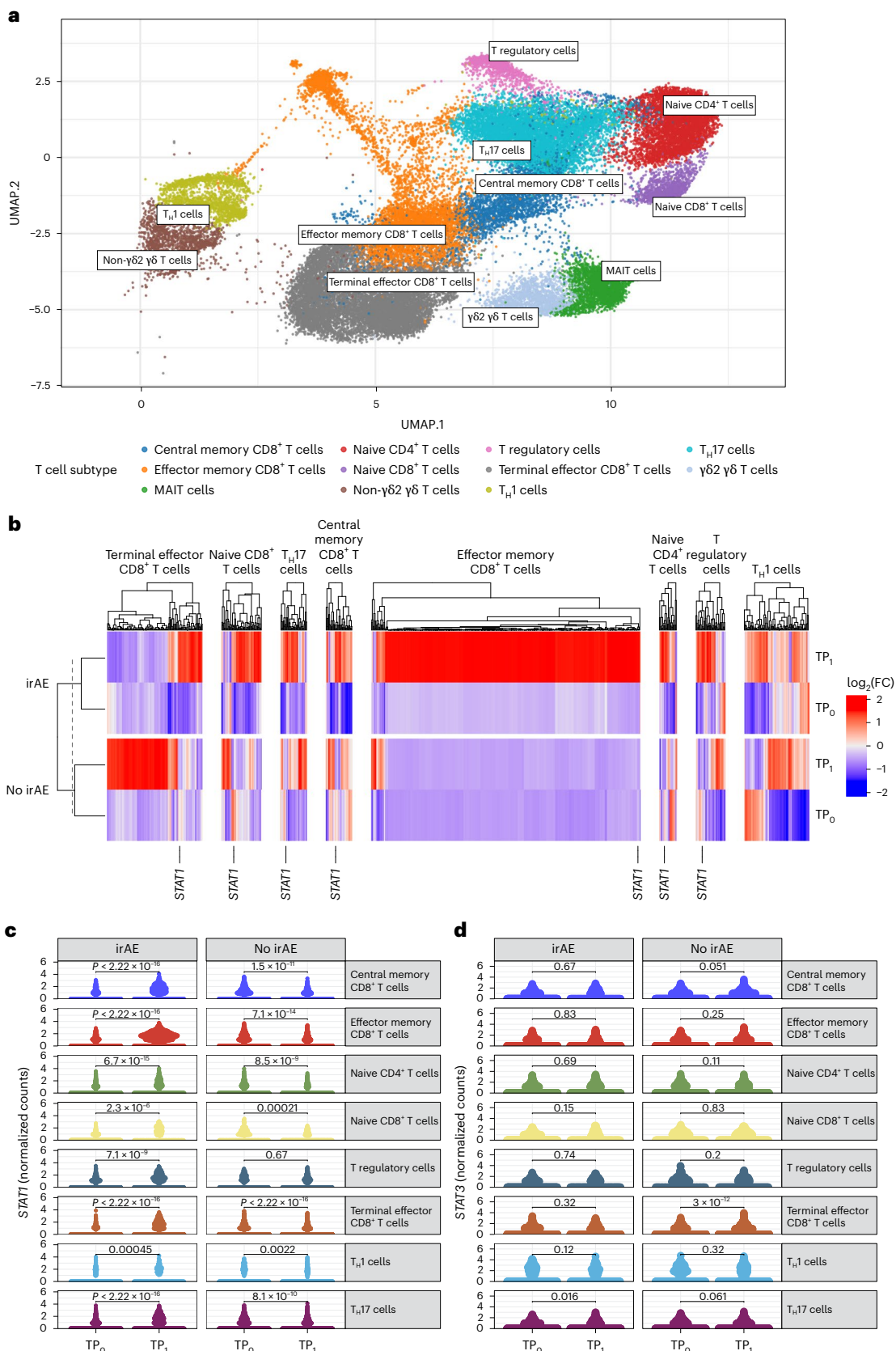


**Fig. 5 | scRNA-seq analysis of the T cell subtypes.** **a**, UMAP plot with overview of the T cell subtypes for the  $n = 6$  patients. **b**, Heatmap with the significantly differentially expressed genes for each T cell subtype at TP<sub>0</sub> and TP<sub>1</sub> for patients with and without irAEs ( $n = 6$ ). **c**, Violin plot of the STAT1 gene for the T cell subtypes between TP<sub>0</sub> and TP<sub>1</sub> ( $n = 6$ ). STAT1 normalized counts between TP<sub>0</sub>

and TP<sub>1</sub> were compared using a two-sided Wilcoxon rank sum test and  $P$  values adjusted by the Benjamini–Hochberg method. **d**, Violin plot of the STAT3 gene for the T cell subtypes between TP<sub>0</sub> and TP<sub>1</sub> ( $n = 6$ ). STAT3 normalized counts between TP<sub>0</sub> and TP<sub>1</sub> were compared using a two-sided Wilcoxon rank sum test and  $P$  values adjusted by the Benjamini–Hochberg method.

involved in the irAEs and to validate the above-mentioned results at the site of the inflamed tissue. Of note, lichenoid skin rashes are the most common dermatologic irAEs in patients treated with ICIs<sup>40</sup>, whereas the incidence of immune-related colitis ranges between 8% and 27%<sup>6</sup>, with diarrhea being a common treatment-related irAE during treatment with ipilimumab and nivolumab treatment<sup>41</sup>. Formalin-fixed, paraffin-embedded (FFPE) skin biopsies from six patients with lichenoid skin rash during treatment with ipilimumab and nivolumab were stained for CD4, CD8, FoxP3, IL-17A, CD68 and pan-cytokeratin (panCK) and compared to normal skin from healthy, consenting individuals obtained through excess skin removal from plastic surgery (Fig. 6a–c). The histopathology reports were reviewed by two independent pathologists. Annotation and quantification of the immune cells was performed with Akoya inForm software (v.2.6.0). Cell classification was based on the protein expression; CD4<sup>+</sup> and IL-17A<sup>+</sup> cells were labeled as T<sub>H</sub>17. A range of 2.3–24.9% cell proportion of IL-17A-producing cells was observed in all six skin rash biopsies compared to 0.3% T<sub>H</sub>17 cells in the normal skin (Fig. 6d). Regulatory T cells were detected in all six skin rash biopsies with a range of 0.2–5.5% cell proportion and were significantly lower in healthy skin (Fig. 6e). In four out of six skin rash biopsies, IL-17A expression was noted in cells positive for panCK with a range of 2.2–14.6% cell proportion. In addition, colon biopsies collected through colonoscopy from five patients with immune-related colitis were compared to normal intestine tissue obtained from healthy individuals during routine colonoscopies (Fig. 6f–h). Similar findings—that is, an increase of T<sub>H</sub>17 and regulatory T cells as well as IL-17A expression—were noted in colon biopsies from patients with ir-colitis compared to normal intestine (Fig. 6i). Specifically, there was a higher expression of CD4<sup>+</sup> and IL-17A<sup>+</sup> cells compared to the normal intestine, with a range of 5.8–20.5% in ir-colitis samples and 0.3–0.7% in normal intestine tissue (Fig. 6j). The abundance of regulatory T cells was increased in patients with ir-colitis, with a range of 3.9–17.2% cell proportion compared to 0.8–2.3% in normal intestine. Collectively, these observations complement the findings in the peripheral blood and show that CD4<sup>+</sup> cells with IL-17A expression are upregulated at the site of the irAE occurrence.

### Spatial transcriptomic analysis in inflamed tissue

To further determine the transcriptomic profile of the cells involved at the site of the irAEs occurrence, we applied a spatial transcriptomic technology on the aforementioned samples of ir-colitis and lichenoid skin rash. Gene expression was measured in FFPE hematoxylin and eosin (H&E)-stained skin and colon sections using Visium technology (10x Genomics). The tissue sections were then spatially resolved in areas (spots) that were equally distributed over the tissue. The generated analysis of the transcriptomes of 4,306 spots and unsupervised clustering by UMAP revealed 11 major cellular clusters that were shared in the inflamed and normal intestine and skin tissue (Fig. 7a). Clusters were defined by their marker gene expression and their spatial location on the analyzed tissue (Fig. 7b). Genes encoding B cells and T cells, as well as T cell checkpoint molecules and macrophages were detected in the different cell types (Fig. 7c). Of note, there were clusters with mixed cell types, such as fibroblasts and epithelial cells, with expression of B cell and T cell markers (CD19, CD8A, IFN $\gamma$ , LAG3) as well as markers from the macrophage lineage, which were identified as fibroblasts

and immune cells' and 'epithelial and immune cells', respectively. Proportion analysis of the identified transcriptomic subpopulations in six lichenoid skin rash biopsies compared to normal skin showed an increase in fibroblasts and immune cells (range, 1–19.5% cell proportion) and T cells and B cells (range, 0.5–40.4% cell proportion) (Fig. 7d). Similar findings were noted in the four colon biopsies of patients with ir-colitis compared to normal intestine; there was an overall increase of epithelial and immune cells (range, 19.9–33.3% versus 0.5% cell proportion), fibroblasts and immune cells (range, 2.7–28.1% versus 0.3% cell proportion) and T cells and B cells (range, 0.3–5.9% versus 0–0.6% cell proportion) (Fig. 7d). The expression of the major identified cell types, as well as the major type I and III cytokines, namely *IFNG*, *IL6* and *IL17A*, was then examined in spatial resolution in the H&E samples (Fig. 8a–p). This analysis showed an enrichment of the main type I and III cytokine transcripts, mainly in the upper dermis layers of the lichenoid skin rash. The respective cytokine transcripts in ir-colitis samples were also unequally distributed across the samples and were significantly enriched in areas of fibroblasts and immune cells, epithelial and immune cells, as well as T cells and B cells. A Wilcoxon rank sum test analysis for the pathway enrichment scores of type I and III cytokine transcripts showed significant differences between normal and inflamed biopsy specimen tissue (all,  $P < 0.01$ ) (Fig. 8q–s). Taken together, these results confirm that cytokine transcripts of type I and III immune responses are present at the site of the irAE occurrence.

### IL-17A blockade for the treatment of severe and refractory irAEs

Based on these results indicating an increase in CD4<sup>+</sup> T cells with IL-17A expression at the site of inflammation, as well as the significant increase of IL-17A from TP<sub>0</sub> to TP<sub>1</sub> in patients with irAEs in all study cohorts, and given the availability of drugs targeting IL-17A, we next reasoned that IL-17A blockade diminishes severe, treatment-refractory irAEs. Therefore, we performed a focused clinical validation in a proof-of-concept case study. Two patients with stage IV melanoma received an anti-IL-17A monoclonal antibody (mAb), secukinumab, for three indications that included lichenoid skin rash grade 3 (according to the Common Terminology Criteria for Adverse Events v.5.0 (CTCAE v.5)), mild immune-related myocarditis (with concomitant immune-related myositis) grade 2 and immune-related colitis grade 3 (Supplementary Table 2). Of note, these irAEs occurred in the context of multiple, concurrent irAEs and were refractory to previous corticosteroid (solumedrol; max. dose of 250 mg day<sup>-1</sup>) and immunomodulatory treatment (TNF inhibitor mAb; max. dose of 5 mg kg<sup>-1</sup> once to twice), as none of these treatments led to resolution of the irAEs of ≤grade 1. Both patients were treated with ipilimumab and nivolumab. The mild immune-related myocarditis was diagnosed based on the typical time window after ICI treatment, recurrence of previous immune-related myocarditis upon ICI re-challenge, elevations of creatine kinase, high-sensitive troponin T (hs-TnT) and I (hs-TnI), mild NT-proBNP increase and positive magnetic resonance imaging criteria. Diagnosis of this mild myocarditis was underlined by an asymptomatic course without electrocardiogram changes or hemodynamic instability. After anti-IL-17A treatment, symptom improvement (≤grade 1) and/or complete resolution of the irAEs was noted within 43 days for the lichenoid skin rash, 20 days for the mild ir-myocarditis and 40 days for the ir-colitis. IL-17A levels were measured

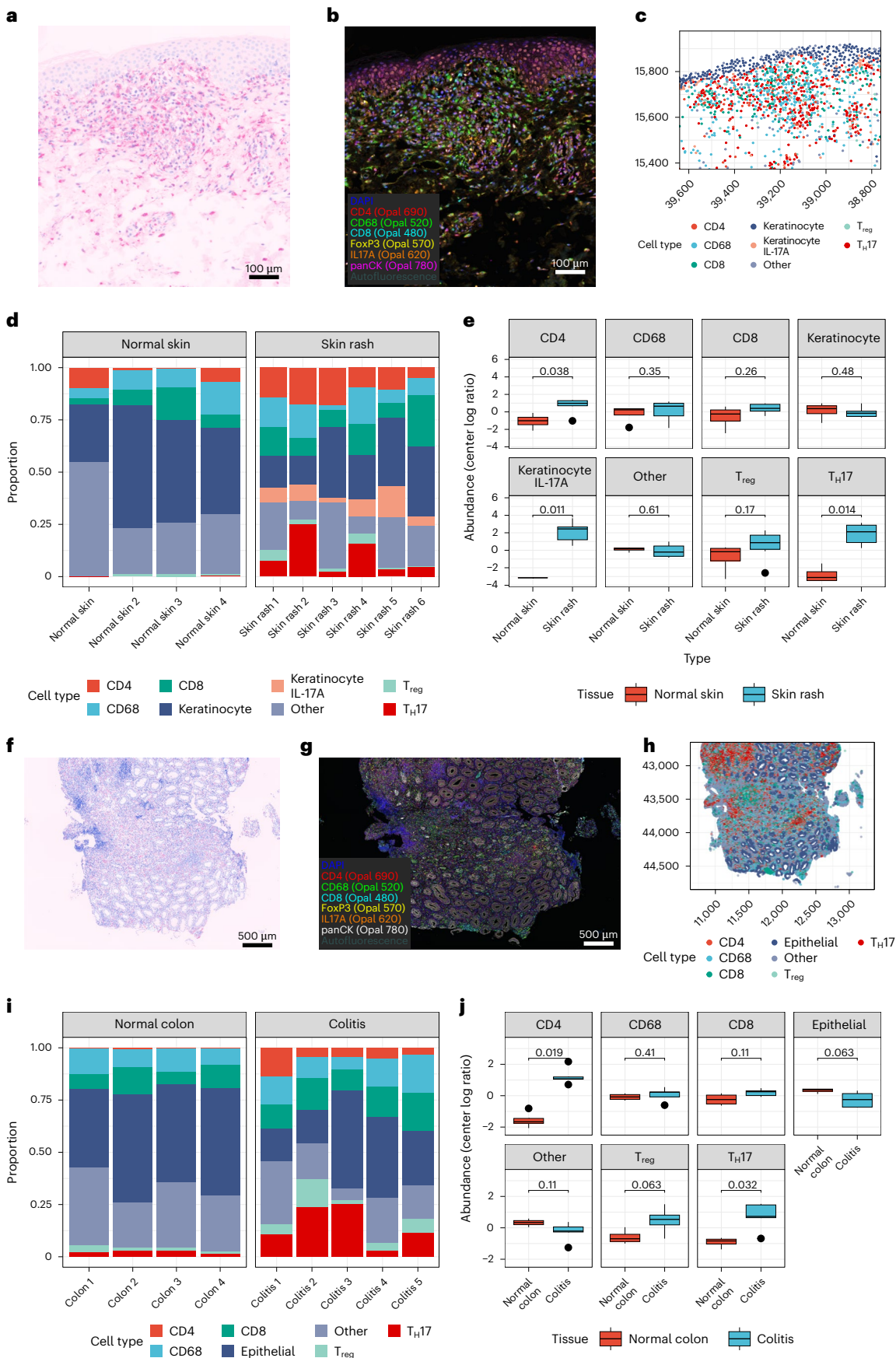
**Fig. 6 | Multiplex immunofluorescence of FFPE tissue samples from biopsies in six patients with lichenoid skin rash and five patients with immune-related colitis.** **a**, H&E staining of a lichenoid skin rash biopsy. **b**, Six-plex immunofluorescence staining for IL-17A, FoxP3, CD4, CD8, CD68 and panCK of a lichenoid skin rash biopsy. **c**, Digital analysis of the multiplex immunofluorescence with cell annotation. T<sub>reg</sub>, regulatory T cell. **d**, Cell proportions of the lichenoid skin rash samples ( $n = 6$ ) compared to normal skin ( $n = 4$ ). **e**, Center log ratio normalized proportions of the lichenoid skin rash samples ( $n = 6$ ) compared to normal skin ( $n = 4$ ). Abundance means were

compared using a two-sided Wilcoxon rank sum test and  $P$  values were not adjusted. **f**, H&E staining of an intestinal biopsy in a patient with ir-colitis.

**g**, Six-plex immunofluorescence of an intestinal biopsy in a patient with ir-colitis.

**h**, Digital analysis of the multiplex immunofluorescence with cell annotation.

**i**, Cell proportions of the ir-colitis samples ( $n = 5$ ) compared to normal intestine ( $n = 4$ ). **j**, Center log ratio normalized proportions of the ir-colitis samples ( $n = 5$ ) compared to normal intestine ( $n = 4$ ). Abundance means were compared using a two-sided Wilcoxon rank sum test and  $P$  values were not adjusted.



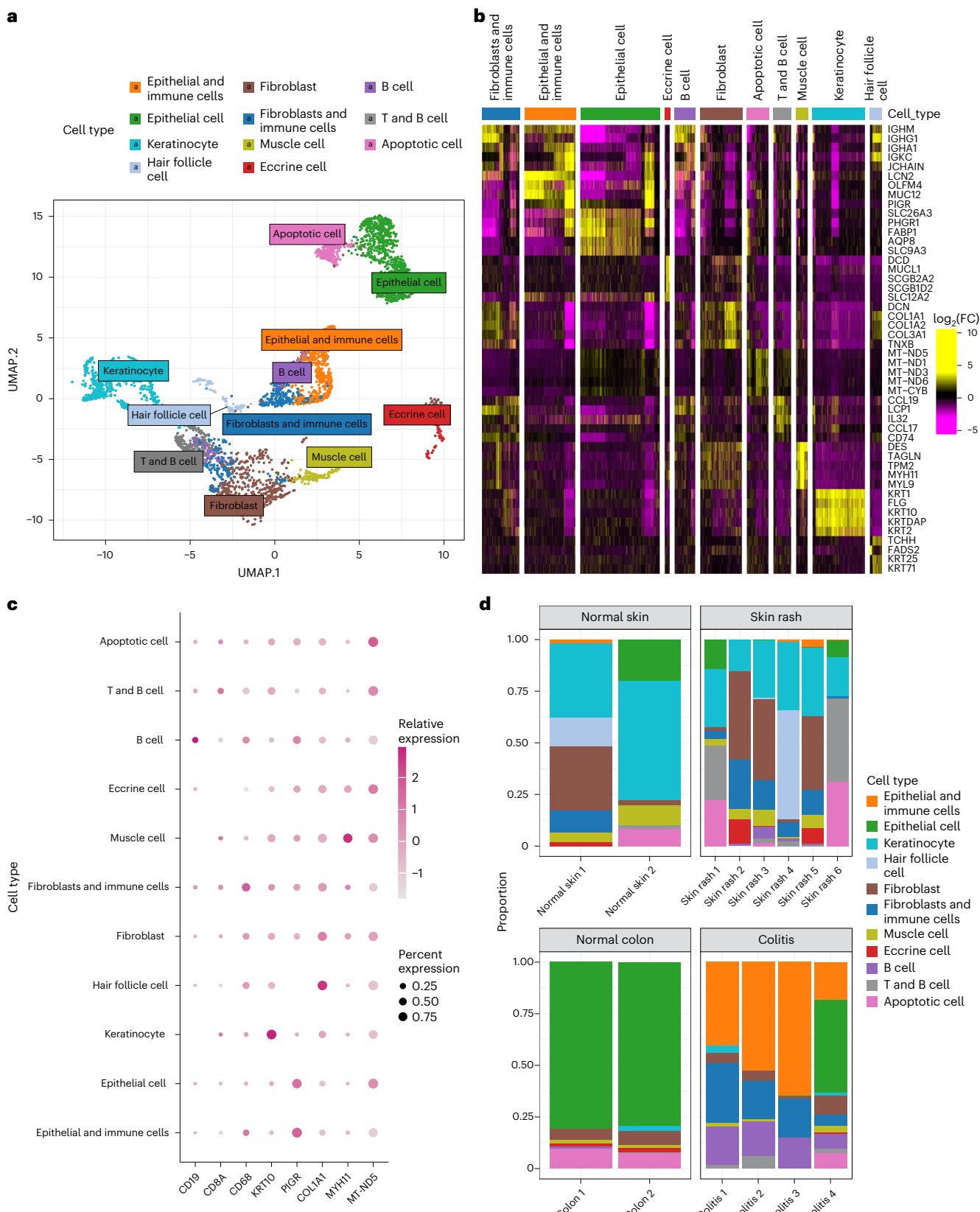


**Fig. 7 | Spatial transcriptomic analysis of lichenoid skin rash ( $n = 6$ ) and immune-related colitis samples ( $n = 4$ ). **a**, UMAP plot with overview of the main cell types of the transcriptomes in the analysis of normal ( $n = 2$ ) and inflamed intestine ( $n = 4$ ), as well as normal ( $n = 2$ ) and inflamed skin tissue ( $n = 6$ ). **b**, Heatmap of the identified clusters and their marker gene expression.**

**c**, Dot plot with gene cell markers, including B cells and T cells (*CD19* and *CD8A*, respectively), macrophages (*CD68*), keratinocytes (*KRT10*), epithelial cells (*PIGR*), fibroblasts (*COL1A1*), myofibroblasts (*MYH11*) and apoptotic cells (*MT-ND5*). **d**, Proportion analysis of the identified transcriptomic subpopulations in inflamed and normal tissue.

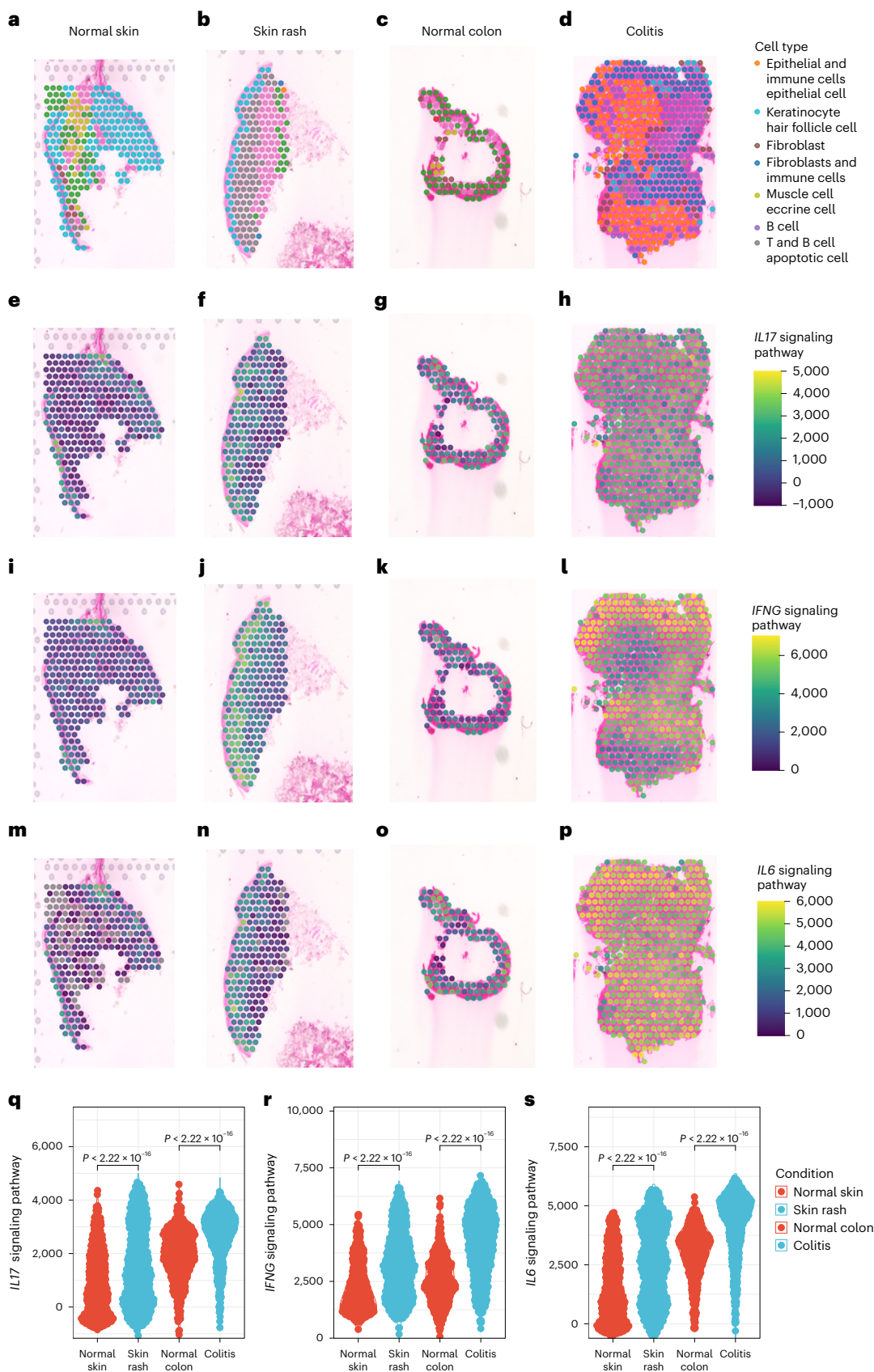


**Fig. 8 | Spatial transcriptomic analysis confirms a cytokine transcript of type I and III immune responses in inflamed tissue.** **a–p.** Representative spatial transcriptomic sections for normal skin (*n* = 2) (a,e,i,m), lichenoid skin rash (*n* = 6) (b,f,j,n), normal colon (*n* = 2) (c,g,k,o) and immune-related colitis samples (*n* = 4) (d,h,l,p) with the major identified cell types and enrichment scores of

signaling pathways of type I and type III immunity. **q–s.** Wilcoxon rank sum test analysis for the pathway enrichment scores of type I and III cytokine transcripts for the IL-17 signaling pathway (q), IFN $\gamma$  signaling pathway (r) and IL-6 signaling pathway (s); each dot represents one spot. The statistical test used was two-sided and *P* values were adjusted by the Benjamini–Hochberg method.

at  $TP_0$  as well as before and after the administration of anti-IL-17A. In the following analysis of available serum samples in these patients, IL-17A increased from  $TP_0$  to the time point before anti-IL-17A administration and decreased after the anti-IL-17A administration in both patients (Extended Data Fig. 7). Secukinumab was administered subcutaneously at a dose of 300 mg weekly for weeks 0–4, followed by 300 mg every 4 weeks. The total number of doses administered was two injections for the treatment of the mild ir-myocarditis and ir-colitis, whereas the patient with the lichenoid skin rash required a 150-day treatment course until complete resolution and discontinuation of secukinumab. The latter did not show any flares or relapses while on treatment and the patient did not require any local corticosteroids. In both patients, treatment with ipilimumab and nivolumab was permanently discontinued. Notably, the first patient was re-challenged with single-agent anti-CTLA4, without flare of the mild ir-myocarditis after a single dose of prophylactic secukinumab given 2 days before anti-CTLA4. The best overall response for the first patient was progressive disease and for the second patient was partial response.

## Discussion

We conducted a translational study to unravel the immune biology of the irAEs induced by ICIs and to propose possible treatment strategies in addition to the standard use of corticosteroids. For that purpose, we designed a prospective study with a precise longitudinal clinical sampling and analysis of serum samples acquired at the time of the irAEs onset. We show aberrant T cell activity with differential expression of type I and III immune signatures in the peripheral serum at the onset of irAEs that differed from the baseline immune signatures. This increase in circulating cytokines was particularly noted in patients with severe (grade  $\geq 3$ ) irAEs and in those with multiple concurrent irAEs. The observed immune signature was in line with an increase in the proportion of CD4 $^+$  T cells with IL-17A expression at the irAEs onset in the peripheral blood using flow cytometry. In contrast to the peripheral blood, multiplex immunofluorescence analysis of human lichenoid skin rash and ir-colitis samples identified a higher than expected proportion of CD4 $^+$  T cells with IL-17A expression. Spatial transcriptomics analysis of the lichenoid skin rash and ir-colitis samples confirmed the notion that type I and III immune responses are involved at the site of the irAE occurrence.

Altogether, and alongside the existing literature evidence, we reason that type I and type III responses are interconnected and that pro-inflammatory T<sub>H</sub>17 cells show double-positive T<sub>H</sub>1/T<sub>H</sub>17 features that are associated with the onset of irAEs in patients treated with ICIs<sup>42,43</sup>. This concept is further supported by the identification of cytokines and chemokines that are induced by IFN $\gamma$ , such as CXCL9 in the peripheral serum. Similar to autoimmune diseases, IL-17-expressing and IFN $\gamma$ -expressing T cells are preferentially found at sites of inflammation<sup>44,45</sup>, whereas after tissue invasion, IL-17-expressing T cells produce high levels of IFN $\gamma$ , indicating a high degree of plasticity<sup>16,43</sup>. Capitalizing on these results, we considered that IL-17A blockade can be used as a therapeutic target to mitigate toxicity in patients with corticosteroid-refractory irAEs. Clinical validation of these results with the administration of anti-IL-17A blockade in two patients who were treated with ipilimumab and nivolumab and who showed a serum increase of IL-17A at the irAEs onset resulted in resolution of severe, treatment-refractory irAEs.

These findings suggest a central role of the type III cells as one of the pathophysiological mechanisms for the development of irAEs. These results are in line with those previously demonstrated in translational studies, showing that expression of IL-6, a T<sub>H</sub>17-cell differentiation cytokine, increased in inflamed, ir-colitis tissue of patients and mice treated with ICIs<sup>20</sup>. In addition, IL-17-producing cells have been linked with the pathogenesis of anti-CTLA4-driven ir-colitis<sup>46,47</sup>, whereas a predominantly T<sub>H</sub>1 phenotype has been identified in ir-colitis and ir-dermatitis tissue in patients treated with ICIs<sup>48</sup>.

Nevertheless, the exact nature of the latter (psoriasiform, lichenoid, maculopapular) has not been accurately defined in the referred study. In accordance with these results, we can show an enrichment of the main type I and (predominantly) type III cytokine transcripts in the spatial analysis, which was prevalent in both lichenoid skin rash and ir-colitis tissue. Respectively, PD1 blockade has been found to shift the antigen-induced cellular reactivity to a T<sub>H</sub>1/T<sub>H</sub>17 response<sup>49</sup>. Notably, although IL-17 is predominantly produced by CD4 $^+$  T cells upon recognition of peptide antigens presented by major histocompatibility complex molecules, several other T cell populations, such as  $\gamma\delta$  T cells and natural killer T cells, have also been shown to produce IL-17, the levels of which are usually low in the peripheral blood<sup>38,39,50</sup>. The differentiation of these cells is also IL-6, TGF- $\beta$  and STAT3-induced<sup>51</sup>. Given that IL-17 has multiple pro-inflammatory properties, it has been previously suggested that selective modulation of the T<sub>H</sub>17 differentiation rather than blocking the IL-17 cytokine per se might be more efficient in the downregulation of this pathway<sup>52</sup>. Further characterization of the immune signature of these IL-17-secreting cells in the context of the ICI-induced irAEs is required to guide personalized treatment decisions in the clinic.

These data underline the association of candidate serum proteins with the development of severe irAEs and may help identify therapeutic targets for their management. It has been previously shown that 11 circulating cytokines, including pro-inflammatory cytokines such as IL-1 $\alpha$ , IL-2 and IFN $\alpha$ 2, could predict the onset of severe irAEs in patients with melanoma that are being treated with anti-PD1-based ICIs<sup>53</sup>. In the current study, CXCL9, and particularly IL-17A, were consistently upregulated and were associated with the onset of irAEs in the main and external validation cohorts (for IL-17A). It has been shown that CXCL9 is induced by IFN $\gamma$ , a type I cytokine<sup>16</sup>, and that IFN $\gamma$  and TNF regulate the expression of CXCL16, which is expressed by colonic myeloid cells in patients with ir-colitis<sup>54</sup>. Additionally, CXCL9, CXCL10 and IFN $\gamma$  are essential in recruiting effector T cells into tumors and have a substantial role in antitumor activity<sup>55</sup>. Similarly, TNF is produced by T<sub>H</sub>1 cells and activated macrophages<sup>56,57</sup>, and increased TNF expression has been found in irAEs cases<sup>20,48</sup>. Taking into consideration the cross-induction of these cytokines, it is suggested to target specific cytokine pathways rather than a single downstream cytokine. In contrast to these type I responses, type III responses are less targeted to distinct immune effector cells<sup>16</sup>. Targeting the IL-17 production could treat ICI-induced toxicity, although its role in antitumor immunity has not yet been clearly specified. A recent study suggested that T<sub>H</sub>17 cytokines support clinical benefit in patients with melanoma being treated with ipilimumab and nivolumab, but not single-agent anti-PD1 (ref. 58). In pancreatic cancer, IL-17 potentiates immunosuppressive effects through the recruitment of tumor-associated neutrophils, and subsequently, higher expression of IL-17 correlates with poorer prognosis<sup>59</sup>. Altogether, there is an inconsistency between the association of IL-17 with the tumor prognosis in the existing literature, which underlines that T<sub>H</sub>17 cells are pleiotropic and their correlation with the treatment response is not linear. Consequently, prospective, randomized studies are required to elucidate the role of anti-IL-17A in the antitumor activity and the control of the irAEs.

We recognize that the present study has limitations. First, the included patients received either single-agent anti-PD1 or dual therapy using ipilimumab and nivolumab. These ICI treatment modalities are associated with different frequencies and severity grades of irAEs. In a phase 3 clinical trial for combined treatment with ipilimumab and nivolumab in advanced melanoma compared to treatment with nivolumab or ipilimumab alone, the type of toxicities did not differ between the two treatment agents<sup>4</sup>. Similarly, in the proteomic analysis of the present study, the changes in log<sub>2</sub>(fold change) at  $TP_0$  and  $TP_1$  were more dependent on the presence (and severity) of the irAEs rather than the treatment type; this observation should be further elucidated in future translational studies. Secondly, a correlation

of these findings with the treatment response to ICIs is not feasible, given that the analyzed samples were specifically collected at the time point of the irAEs onset, and the median time from treatment initiation to serum collection was longer in patients with irAEs than in those without irAEs (37 days versus 22 days for the main and the internal validation cohorts). In addition, the heterogeneity of the tumor stages, treatment types, timing and type of investigations as well as the concurrent administration of corticosteroids and other immunosuppressive agents are not yet standardized and remain challenges in this analysis. Even though a positive correlation between tumor response to ICIs and increased risk for development of irAEs has been observed in randomized clinical and translational studies<sup>60,61</sup>, it remains unclear whether the timing of the onset of irAEs coincides with the response onset. We additionally recognize that some of the investigated proteins increased over time in patients without irAEs, and although these changes were not significant in the present study, this analysis is limited by the smaller sample size of these patients. Furthermore, in contrast to previous reports<sup>53,62</sup>, this study was not designed to identify predictive biomarkers for stratification of patients at risk for the development of irAEs, although its findings may support future experimental studies to further investigate their predictive value. Moreover, cytokine release in peripheral blood is transient and therefore poorly captured by most immunological assays, including scRNA-seq<sup>63</sup>. Similarly, T<sub>H</sub>17 cells comprise only a small fraction of cells in the peripheral blood<sup>64</sup>. Lastly, the cytokine functions are pleiotropic and depend on the cell-type-specific receptor usage, such that characterization of these signaling activities at a single-cell level might be challenging<sup>65</sup>.

In conclusion, this study highlights the association of type III CD4<sup>+</sup> T cells in the irAE development and provides proof-of-principle evidence to support a clinical trial examining anti-IL-17A for the management of irAEs. The differential expression of type I and III immune signatures in the peripheral serum at the irAEs onset, in particular in patients with severe (grade  $\geq 3$ ) irAEs or those with multiple concurrent irAEs early during the treatment course, emphasizes that these patients should be differentially classified and treated. The increase in the proportion of CD4<sup>+</sup> T cells with IL-17A expression at the site of the inflammation suggests a key role of the type III responses across barrier tissues. Inhibiting these central inflammatory components may represent a more specific and effective therapeutic approach for the management of irAEs in addition to corticosteroid use. Correlative studies investigating the effect of anti-IL-17A in the antitumor response in a prospective, randomized setting will further highlight the multifunctional role of the T<sub>H</sub>17 pathway in patients with melanoma treated with ICIs and will determine whether this approach is superior to other treatment strategies.

## Methods

### Ethics approval and consent to participate

Informed consent was obtained from all patients and healthy tissue donors, and all study analyses conformed to the principles set out in the World Medical Association Declaration of Helsinki and the Department of Health and Human Services Belmont Report. Healthy abdominal skin was obtained from consenting adult individuals and provided by the plastic surgery department of the University Hospital of Zurich with the assistance of the SKINTEGRITY.CH biobank. PBMCs and serum from patients were collected by the University Research Priority Program Cancer Biobank. The use of material for research purposes was approved by the Zurich Cantonal Ethic Commission (KEK-Nr. 2020-01148 and KEK-Nr. 2017-00688) and the ethics committee of Hannover Medical School (Nr. 8685\_BO\_K\_2019). The study was conducted in accordance with the Declaration of Helsinki guidelines.

The anti-IL-17A treatment was approved and reimbursed by the Federal Office of Public Health through a specific allowance in the Swiss health codes (article 71a KVV, from 27 June 1995). More information about Article 71a can be found on the website of the Swiss Department

of Health (<https://www.bag.admin.ch/bag/en/home/versicherungen/krankenversicherung/krankenversicherung-leistungen-tarife/Arzneimittel/vergütung-ärzneimittel-im-einzelfall.html>).

### Study population and clinical samples

We included patients with advanced, stage III–IV (AJCC v.8)<sup>66</sup> melanoma treated with anti-PD1-based treatment in the Department of Dermatology at the University Hospital of Zurich. Patients received either nivolumab (240 mg every 2 weeks), pembrolizumab (200 mg every 3 weeks), or combination of nivolumab and ipilimumab (1 mg kg<sup>-1</sup> nivolumab and 3 mg kg<sup>-1</sup> ipilimumab every 3 weeks, followed by nivolumab monotherapy 240 mg every 2 weeks). Patients were treated in the metastatic setting. Previous treatments were allowed; however, irAEs from previous treatments had to be completely resolved or be  $\leq$  grade 1 at the time of the treatment initiation for inclusion in the study. Overall, previous ongoing irAEs were noted in four (5%) patients of the main study cohort and included immunotherapy-induced hypothyroidism as a result of previous immune-related thyroiditis in two patients, immune-related uveitis in one patient and immune-related hepatitis in one patient, with a flare of the immune-related hepatitis upon ICI re-challenge. The discovery cohort was chosen from a retrospective cohort of 53 patients treated between January 2017 and August 2020, with available blood samples at baseline and the onset of the irAE. For the final analysis of the discovery cohort, nine patients with severe ( $\geq$  grade 3, CTCAE v.5) irAEs that occurred early during the treatment and with available blood samples at baseline (0–29 days before therapy initiation) and at the irAEs onset were chosen. The discovery cohort was used as an exploratory cohort for the correlation of specific cytokines and chemokines with the irAEs onset.

The main study cohort was derived after the establishment of a study protocol with a prospective sample collection in patients treated with anti-PD1-based ICIs, including both single-agent anti-PD1 (pembrolizumab and nivolumab) and anti-PD1 in combination with anti-CTLA4 (ipilimumab). In this prospective study cohort, blood samples were prospectively collected at baseline (0–29 days before therapy initiation) and at regular intervals during therapy from August 2019 to March 2021. For the final analysis of the prospective study cohort, blood samples at baseline (0–29 days before therapy initiation) and at the irAEs onset or at the second to fifth infusion (in patients without any irAEs) were chosen.

An independent external validation cohort of patients with advanced, stage III–IV (AJCC v.8) melanoma started ICI treatment from October 2019 to February 2022 in the Department of Dermatology at Medical School Hannover was used to validate these results. Patients received either anti-PD1-based monotherapy (nivolumab) or a combined treatment with nivolumab and anti-CTLA-4 (ipilimumab). Blood samples taken at baseline and at irAEs onset or at the second to fifth infusion (in patients without any irAEs) were chosen. All serum samples were separated at 1,500 g for 10 min and the extracted serum was stored at  $-80^{\circ}\text{C}$  until further analysis. Patient demographics and clinicopathologic features included sex, age, disease stage (AJCC v.8), baseline lactate dehydrogenase (LDH) and Eastern Cooperative Oncology Group (ECOG) performance status for prior therapy were collected. Treatment characteristics, including investigator-assessed treatment response, were assessed radiologically at regular time intervals and according to the RECIST 1.1 criteria. Patients who achieved complete or partial response or stable disease were defined as ‘responders’. Toxicity data were assessed using CTCAE v.5. Follow-up duration was calculated from the date of treatment initiation to the date of death, loss of follow-up or December 2022 (data cutoff).

Patient demographics and clinicopathologic features were collected for all patients included in the study. These included sex, age, disease stage (AJCC v.8), baseline LDH, previous treatments as well as the presence of autoimmune disease and ongoing toxicities from previous treatments at the treatment initiation. Treatment characteristics,

including investigator-assessed treatment response, were assessed radiologically at regular time intervals and according to the RECIST 1.1 criteria<sup>67</sup>. Patients who achieved complete or partial response or stable disease for >6 months after treatment initiation were defined as ‘responders’. The best overall response was evaluated per the last available follow-up. Toxicity data were assessed using CTCAE v.5. Follow-up duration was calculated from the date of the treatment initiation to the date of death, loss of follow-up or August 2022 (data cutoff).

### Blood samples

Blood samples, including serum and PBMCs, were collected at baseline (0–29 days before therapy initiation) and at regular time points during the therapy, until cycle 4. In the case of an irAE after cycle 4, additional blood samples were collected at irAE onset.

### Multiplex cytokine–chemokine assay

Undiluted serum samples were profiled using the U-PLEX Assay Platform (MSD), as previously described<sup>68</sup>. In brief, biotinylated capture antibodies are coupled to U-PLEX linkers, which self-assemble onto unique spots on the U-PLEX plate. Analytes in the sample bind to the capture reagents; detection antibodies conjugated with electrochemiluminescent labels (MSD GOLD SULFO-TAG) bind to the analytes to complete the sandwich immunoassay. Once the sandwich immunoassay is complete, the U-PLEX plate is loaded into an MSD instrument, where a voltage applied to the plate electrodes causes the captured labels to emit light. The instrument measures the intensity of emitted light (which is proportional to the amount of analyte present in the sample) and provides a quantitative measure of each analyte in the sample. Each run was performed in duplicate for the discovery cohort; duplicates did not vary by more than 4%. A customized U-PLEX assay for the analysis of the following cytokines and chemokines was used in the discovery cohort: eotaxin, fractaline (CX3CL1), G-CSF, GM-CSF, IFN $\alpha$ 2a, IFN $\beta$ , IFN $\gamma$ , IL-1 $\alpha$ , IL-1 $\beta$ , IL-2, IL-3, IL-4, IL-5, IL-6, IL-8, IL-9, IL-10, IL-12p70, IL-13, IL-17A, IL-18, IL-21, IL-22, IL-23, IP-10, I-TAC, MCP-1, MIP-1 $\alpha$ , MIP-1 $\beta$ , TNF, TNF $\beta$  (LTA), VEGF-A and VEGF-D. For the main study cohort, the same assay without IL-3, IL-9, IL-13 and VEGF-D was used. For the external cohort, a V-Plex assay according to the manufacturer’s instructions was applied. Data were collected by the Discovery Workbench v.4.0 (MSD).

### Olink proteomics

Proteome analysis of baseline and on-treatment serum samples from the main study and internal validation cohort has been carried out using the Olink Explore 384 Inflammation panel (Olink Proteomics). Data collection was performed by Olink. This panel provides a high-throughput, multiplex immunoassay enabling analysis of 384 inflammation-related protein biomarkers across 96 samples simultaneously, using the proximity extension assay technology, as previously described<sup>69</sup>. In brief, pairs of oligonucleotide-labeled antibody probes bind to their targeted protein, and if the two probes are brought in proximity, the oligonucleotides will hybridize in a pair-wise manner. The addition of a DNA polymerase leads to a proximity-dependent DNA polymerization event, generating a unique target sequence analyzed through either next-generation sequencing or real-time PCR. Data were quality controlled and normalized using an internal extension control and an inter-plate control, to adjust for intra-run and inter-run variation. The final assay read-out is presented in NPX values, which is an arbitrary unit on a log<sub>2</sub> scale in which a high value corresponds to a higher protein expression. All assay validation data are available on the manufacturer’s website ([www.olink.com](http://www.olink.com)).

### Multiplex immunofluorescence

BOND RXm fully automated staining system was used in conjunction with the Opal Polaris 7-Color Automated IHC Detection Kit (NEL871001KT, Akoya Biosciences) according to user manual instructions. All antibodies were used at a dilution of 1:100 (IL-17A: ab79056,

Abcam; FoxP3: 14-4777-82, Invitrogen, eBioscience; CD4: ab133616, Abcam; CD8: ab4055, Abcam; CD68: ab213363, Abcam; panCK: sc-8018, Santa Cruz Biotechnology). Slides were imaged simultaneously using the PerkinElmer Vectra Polaris imaging system maintained by the Center for Microscopy and Image Analysis, University of Zurich. Slide visualization and regions of interest selection were performed in Phenochart whole-slide viewer (Akoya Biosciences). Whole-slide scans can be made available on reasonable request. Cell segmentation training was performed according to DAPI nuclear staining, followed by cell marker phenotyping (CD4, CD8, CD68, FoxP3, IL-17A and panCK). Data were collected with InForm v.2.6.0 (Akoya Biosciences). In-depth spatial expression analysis was performed using Giotto (v.2.0.0.957)<sup>70</sup>.

### scRNA-seq sample processing

Live cell biobanked PBMC samples were quickly thawed in a water bath set to 37 °C, re-suspended in 10 ml ice-cold RPMI (Sigma-Aldrich, cat. no. R0883) with 0.04% BSA (Sigma-Aldrich, cat. no. A7906) and incubated for 10 min on ice to allow the dimethylsulfoxide to diffuse from the tissue. Samples were spun down at 300g for 5 min and re-suspended in PBS with 0.04% BSA (Sigma-Aldrich, cat. no. A7906); cell count and viability were assessed using Luna-FL cell counter (Dual Fluorescence Cell Counter, Logos Biosystems, cat. no. L1001) using acridine orange propidium iodide (Logos Biosystems, cat. no. F23001) live/dead staining. Cell concentration was set according to 10x Genomics recommendation to 700–1,000 cells per  $\mu$ l; 10,000 cells were targeted per sample. Cell suspensions were loaded on Chip K (10x Genomics, PN-1000286) and processed using the 10x Genomics Chromium platform with the SPV(D)J immune profiling kit v.2 on a 10x Genomics Chromium Single Cell Controller (10x Genomics, PN-120263). Gene expression libraries were amplified and sequenced on the Illumina NovaSeq 6000 platform at recommended sequencing depth (20,000–30,000 reads per cell for GEX libraries).

### scRNA-seq analysis

Raw sequencing data were processed using the 10x Chromium Cell Ranger pipeline (v.7.0.0) (<https://support.10xgenomics.com/single-cell-gene-expression/software/downloads/latest>). Reads were aligned to the human reference genome (GRCh38, 2020-A) (10x Genomics). Single cells were filtered with the following parameters; >500 genes and <9,000 genes detected, <40% mitochondrial RNA and defined as ‘singlet’ by scDblFinder v.1.18.0 (ref. 71). The Seurat v.4 pipeline using SCTransform was used to normalize gene expression data<sup>72</sup>. Data integration was performed using 3,000 most variable features and the reciprocal PCA method using 30 dimensions. Dimension reduction was performed with PCA, followed by Leiden clustering using a resolution of 2.5. Visualization onto two-dimensional space was performed with UMAP. Cell typing was performed with SingleR<sup>73</sup> (v.1.4.1) using the Monaco Immune dataset ([GSE107011](https://www.ncbi.nlm.nih.gov/geo/query/acc.cgi?acc=GSE107011); PMID: 30726743). Differential expression was performed with the FindMarkers function from the Seurat v.4 package. ggplot2 (v.3.5.0) was used for visualizing aggregated data.

### Cell stimulation and intracellular cytokine staining for flow cytometry

Live cell biobanked PBMC samples were quickly thawed in a water bath set to 37 °C, re-suspended in 10 ml of warm RPMI-1640 (Sigma-Aldrich, cat. no. R0883) supplemented with 5 nM L-glutamine (Gibco, Thermo Scientific, cat. no. 25030-024), 1 mM sodium pyruvate (Sigma-Aldrich, cat. no. S8636), 10% heat-inactivated fetal bovine serum (Biowest, cat. no. S181H) and 1% penicillin–streptomycin (Gibco, Thermo Scientific, cat. no. 15140-122). Cells were seeded in round-bottom 96-well plates at  $1 \times 10^6$  cells per well (or less when not enough cells were available) and stimulated with Cell Stimulation Cocktail plus protein transport inhibitors (ThermoFisherScientific, cat. no. 00-4975-93) for 4 h at 37 °C with 5% CO<sub>2</sub>.

For flow cytometry staining, the cells were first stained with a fixable viability dye (Zombie Aqua, BioLegend, cat. no. 423101) according to the manufacturer's instructions. Cells were washed with PBS + 2% FCS and stained with the following surface antibodies: CD3 APC (BioLegend, cat. no. 317318), CD4 Alexa Fluor 700 (BioLegend, cat. no. 344621), CD19 FITC (BioLegend, cat. no. 302205), CD8 Brilliant Violet 711 (BioLegend, cat. no. 344733), TCRγδ PE (BioLegend, cat. no. 331209) and HLA-DR Pacific Blue (BioLegend, cat. no. 307623). After surface staining, cells were washed with PBS + 2% FCS, and intracellular staining was performed using the Cyto-Fast Fix/Perm Buffer Set (BioLegend, cat. no. 426803) according to the manufacturer's instructions and anti-human IL-17A PE-Cy7 (BioLegend, cat. no. 512315) or Mouse IgG1, κ Isotype Ctrl Antibody PE/Cy7 (BioLegend, cat. no. 400125) at the same concentration. Samples were acquired on an LSRFortessa Cell Analyzer (BD Biosciences), and data were analyzed with FlowJo (v.10.8.1).

### Spatial transcriptomics Visium library preparation and sequencing

Sample processing and library preparation were performed according to the 10x Genomics manuals for Visium CytAssist Spatial Gene Expression for FFPE, using the human probe set v.2 and Visium slides with 6.5-mm capture areas. In short, FFPE samples were sectioned to 5-μm thickness and placed on Superfrost Plus slides. Sections were deparaffinized, H&E-stained and imaged on a Roche Ventana DP 200 Slide Scanner followed by destaining, decrosslinking and 16 h of probe hybridization. Ligated probes were transferred to Visium slides using the CytAssist instrument with standard parameters (37 °C and 30 min). Quality control was performed on the Roche LightCycler 96 for pre-amplified libraries and on the Agilent 4200 Tapestation for the final indexed libraries.

### Spatial transcriptomics sequencing

The libraries were pooled according to estimated Visium slide coverage (Loupe Browser, 10x Genomics) and paired-end sequenced on an Illumina NovaSeq 6000 platform (Sequencing configuration: read1, 28; i7-index, 10; i5-index, =10; read 2, 91) using an S1 flowcell (100 cycles).

### Spatial Visium analysis

Raw sequencing data were processed using the 10x Chromium SpaceRanger pipeline (v.2.0.0) (<https://support.10xgenomics.com/spatial-gene-expression/software/downloads/latest>). Reads were aligned to the human reference genome (GRCh38, 2020-A) (10x Genomics). Spots with fewer than ten genes were filtered out. The Seurat v.4 pipeline for spatial analysis using SCTransform was used to normalize the data. Dimension reduction was performed with PCA, and clustering was performed with FindNeighbors and FindClusters using default parameters. Data integration was performed with Harmony<sup>74</sup>. Clusters were annotated manually from markers defined by FindAllmarkers. Gene set enrichment was performed using the package 'escape'.

### Statistical analysis

Clinical data were analyzed using gtsummary (v.1.7.2). For analysis of the clinical data, continuous variables (for example, age and follow-up time) were compared with a Student's *t*-test or Wilcoxon rank test, as appropriate. Categorical variables (for example, sex, stage and LDH) were analyzed with a chi-squared test or Fisher's exact test, as appropriate. All statistical tests used were two-sided. The Benjamini–Hochberg method was used for multiple testing correction. A *P* value of <0.05 was deemed statistically significant.

For the analysis of the multiplex cytokine–chemokine assay, MSD electrochemiluminescence data were imported into the MSD Discovery Workbench (v.4.0) analysis software for quantification. Quantified serum proteins were then imported into R (v.4.3.0) for statistical analysis. A linear mixed model was used to evaluate differences in serum proteins between the samples with and without adverse events in

association with the time of the adverse event onset and the treatment response and between TP<sub>1</sub> and TP<sub>0</sub>. Differences in the log<sub>2</sub>(fold changes) between TP<sub>1</sub> (time of the irAEs onset of second to fifth infusion) and TP<sub>0</sub> (baseline) were evaluated with the Wilcoxon rank test and corrected for multiple testing with the Benjamini–Hochberg method. A *P* value of <0.05 was deemed statistically significant.

For the analysis of the proteomic data, Olink proteomic data were imported with the OlinkAnalyze R package (v.3.7.0). Differences in the log<sub>2</sub>(fold changes) between TP<sub>1</sub> and TP<sub>0</sub> were evaluated with the Wilcoxon rank test and corrected for multiple testing with the Benjamini–Hochberg method. A linear mixed model was used to evaluate differences in serum proteins between the samples with and without adverse events in association with the time of the adverse event onset and the treatment response and between TP<sub>1</sub> and TP<sub>0</sub>. The Benjamini–Hochberg method was used for multiple testing correction. A *P* value of <0.05 was deemed as statistically significant.

For the multiplex immunofluorescence and the spatial transcriptomic analysis, centered log ratios were compared using a two-sided Wilcoxon rank sum test and *P* values were adjusted with the Benjamini–Hochberg method. For flow cytometry, significant differences in the cell proportion analyses were determined by a one-sided Wilcoxon rank sum test.

### Statistics and reproducibility

No statistical methods were used to pre-determine sample sizes, but our sample sizes are similar to those reported in previous publications<sup>53</sup>. No data were excluded from the analyses. This is an observational study and data collection was not randomized. Experiments involving Olink proteomic data, scRNA-seq, multiplex immunofluorescence and spatial transcriptomics were performed once. For the multiplex cytokine–chemokine assay (MSD), each run was performed in duplicate for the discovery cohort; duplicates did not vary by more than 4%. The flow cytometry experiment was performed in three replicates. All techniques and reagents used for the analyses of this study were previously optimized and validated. The investigators were not blinded to allocation during experiments and outcome assessment. Data collection and analysis were not performed blind to the conditions of the experiments. The data were formally tested for normality and equal variances and did not pass. Thus, non-parametric tests, such as the Wilcoxon rank-sum test, were used to compare groups. Further information on research design is available in the Nature Research Reporting Summary linked to this article.

### Subject details

Participant information on gender and age was self-reported. Information regarding gender, race and socioeconomic status was not collected. Patient information including gender and age are reported in Supplementary Table 1. Consent has been obtained for reporting and sharing individual-level data.

### Reporting summary

Further information on research design is available in the Nature Portfolio Reporting Summary linked to this article.

### Data availability

The data supporting the findings of this study are available within the manuscript. The scRNA-seq and Visium-aligned 10x single-cell files that support the findings of this study are available at <https://doi.org/10.5281/zenodo.10390377>. Source data for Figs. 2, 3 and 5, as well as Extended Data Figs. 1, 2, 3, 6 and 7 have been provided as Source Data files. All other relevant de-identified raw data related to the current study are available from the corresponding authors upon reasonable academic request and will require the researcher to sign a data access agreement with the University Hospital of Zurich. Individual patient-identifiable data are not available owing

to concerns with patient identification. Source data are provided with this paper.

## Code availability

Code to generate the figures is available at the GitHub repository [https://github.com/pcheng84/AE\\_analysis](https://github.com/pcheng84/AE_analysis).

## References

- Postow, M. A., Callahan, M. K. & Wolchok, J. D. Immune checkpoint blockade in cancer therapy. *J. Clin. Oncol.* **33**, 1974–1982 (2015).
- Postow, M. A., Sidlow, R. & Hellmann, M. D. Immune-related adverse events associated with immune checkpoint blockade. *N. Engl. J. Med.* **378**, 158–168 (2018).
- Robert, C. et al. Pembrolizumab versus ipilimumab in advanced melanoma. *N. Engl. J. Med.* **372**, 2521–2532 (2015).
- Larkin, J. et al. Combined nivolumab and ipilimumab or monotherapy in untreated melanoma. *N. Engl. J. Med.* **373**, 23–34 (2015).
- Haanen, J. et al. Management of toxicities from immunotherapy: ESMO clinical practice guideline for diagnosis, treatment and follow-up. *Ann. Oncol.* **33**, 1217–1238 (2022).
- Schneider, B. J. et al. Management of immune-related adverse events in patients treated with immune checkpoint inhibitor therapy: ASCO guideline update. *J. Clin. Oncol.* **39**, 4073–4126 (2021).
- Ghisoni, E. et al. Late-onset and long-lasting immune-related adverse events from immune checkpoint-inhibitors: an overlooked aspect in immunotherapy. *Eur. J. Cancer* **149**, 153–164 (2021).
- Wang, D. Y. et al. Fatal toxic effects associated with immune checkpoint inhibitors: a systematic review and meta-analysis. *JAMA Oncol.* **4**, 1721–1728 (2018).
- Johnson, D. B. et al. Fulminant myocarditis with combination immune checkpoint blockade. *N. Engl. J. Med.* **375**, 1749–1755 (2016).
- Teulings, H. E. et al. Vitiligo-like depigmentation in patients with stage III–IV melanoma receiving immunotherapy and its association with survival: a systematic review and meta-analysis. *J. Clin. Oncol.* **33**, 773–781 (2015).
- Axelrod, M. L. et al. T cells specific for  $\alpha$ -myosin drive immunotherapy-related myocarditis. *Nature* **611**, 818–826 (2022).
- Caturegli, P. et al. Hypophysitis secondary to cytotoxic T-lymphocyte-associated protein 4 blockade: insights into pathogenesis from an autopsy series. *Am. J. Pathol.* **186**, 3225–3235 (2016).
- Iwama, S. et al. Pituitary expression of CTLA-4 mediates hypophysitis secondary to administration of CTLA-4 blocking antibody. *Sci. Transl. Med.* **6**, 230ra245 (2014).
- Sullivan, R. J. & Weber, J. S. Immune-related toxicities of checkpoint inhibitors: mechanisms and mitigation strategies. *Nat. Rev. Drug Discov.* **21**, 495–508 (2022).
- Das, R. et al. Early B cell changes predict autoimmunity following combination immune checkpoint blockade. *J. Clin. Invest.* **128**, 715–720 (2018).
- Tuzlak, S. et al. Repositioning T<sub>H</sub> cell polarization from single cytokines to complex help. *Nat. Immunol.* **22**, 1210–1217 (2021).
- O'Connor, W. Jr. et al. A protective function for interleukin 17A in T cell-mediated intestinal inflammation. *Nat. Immunol.* **10**, 603–609 (2009).
- Sonnenberg, G. F. et al. Pathological versus protective functions of IL-22 in airway inflammation are regulated by IL-17A. *J. Exp. Med.* **207**, 1293–1305 (2010).
- Conti, H. R. et al. T<sub>H</sub>17 cells and IL-17 receptor signaling are essential for mucosal host defense against oral candidiasis. *J. Exp. Med.* **206**, 299–311 (2009).
- Hailemichael, Y. et al. Interleukin-6 blockade abrogates immunotherapy toxicity and promotes tumor immunity. *Cancer Cell* **40**, 509–523.e6 (2022).
- Tarhini, A. A. et al. Baseline circulating IL-17 predicts toxicity while TGF- $\beta$ 1 and IL-10 are prognostic of relapse in ipilimumab neoadjuvant therapy of melanoma. *J. Immunother. Cancer* **3**, 39 (2015).
- Dimitriou, F., Hogan, S., Menzies, A. M., Dummer, R. & Long, G. V. Interleukin-6 blockade for prophylaxis and management of immune-related adverse events in cancer immunotherapy. *Eur. J. Cancer* **157**, 214–224 (2021).
- Stroud, C. R. et al. Tocilizumab for the management of immune mediated adverse events secondary to PD-1 blockade. *J. Oncol. Pharm. Pract.* **25**, 551–557 (2019).
- Tokunaga, R. et al. CXCL9, CXCL10, CXCL11/CXCR3 axis for immune activation—a target for novel cancer therapy. *Cancer Treat. Rev.* **63**, 40–47 (2018).
- Yao, Z. et al. Human IL-17: a novel cytokine derived from T cells. *J. Immunol.* **155**, 5483–5486 (1995).
- Ladolce, J. P., Burkett, P. R., Koka, R. M., Boone, D. L. & Ma, A. Regulation of lymphoid homeostasis by interleukin-15. *Cytokine Growth Factor Rev.* **13**, 429–439 (2002).
- Lamy, P. J. et al. Quantification and clinical relevance of gene amplification at chromosome 17q12-q21 in human epidermal growth factor receptor 2-amplified breast cancers. *Breast Cancer Res.* **13**, R15 (2011).
- Kontos, F. et al. B7-H3: an attractive target for antibody-based immunotherapy. *Clin. Cancer Res.* **27**, 1227–1235 (2021).
- Boyman, O. & Sprent, J. The role of interleukin-2 during homeostasis and activation of the immune system. *Nat. Rev. Immunol.* **12**, 180–190 (2012).
- Borst, J., Hendriks, J. & Xiao, Y. CD27 and CD70 in T cell and B cell activation. *Curr. Opin. Immunol.* **17**, 275–281 (2005).
- Hayette, S. et al. FLRG (follistatin-related gene), a new target of chromosomal rearrangement in malignant blood disorders. *Oncogene* **16**, 2949–2954 (1998).
- Karsunky, H., Merad, M., Cozzio, A., Weissman, I. L. & Manz, M. G. Flt3 ligand regulates dendritic cell development from Flt3<sup>+</sup> lymphoid and myeloid-committed progenitors to Flt3<sup>+</sup> dendritic cells in vivo. *J. Exp. Med.* **198**, 305–313 (2003).
- Al-Obaide, M. A., AlObaydi, H., Abdelsalam, A. G., Zhang, R. & Srivenugopal, K. S. Multifaceted roles of 5'-regulatory region of the cancer associated gene B4GALT1 and its comparison with the gene family. *Int. J. Oncol.* **47**, 1393–1404 (2015).
- Maglione, D. et al. Two alternative mRNAs coding for the angiogenic factor, placenta growth factor (PIGF), are transcribed from a single gene of chromosome 14. *Oncogene* **8**, 925–931 (1993).
- Platchek, M., Lu, Q., Tran, H. & Xie, W. Comparative analysis of multiple immunoassays for cytokine profiling in drug discovery. *SLAS Discov.* **25**, 1197–1213 (2020).
- Zweig, M. H. & Campbell, G. Receiver-operating characteristic (ROC) plots: a fundamental evaluation tool in clinical medicine. *Clin. Chem.* **39**, 561–577 (1993).
- Cui, W., Liu, Y., Weinstein, J. S., Craft, J. & Kaech, S. M. An interleukin-21-interleukin-10-STAT3 pathway is critical for functional maturation of memory CD8<sup>+</sup> T cells. *Immunity* **35**, 792–805 (2011).
- Akitsu, A. & Iwakura, Y. Interleukin-17-producing  $\gamma\delta$  T ( $\gamma\delta$ 17) cells in inflammatory diseases. *Immunology* **155**, 418–426 (2018).
- Veldhoen, M. Interleukin 17 is a chief orchestrator of immunity. *Nat. Immunol.* **18**, 612–621 (2017).
- Apalla, Z. et al. European recommendations for management of immune checkpoint inhibitors-derived dermatologic adverse events. The EADV task force ‘Dermatology for cancer patients’ position statement. *J. Eur. Acad. Dermatol. Venereol.* **36**, 332–350 (2022).

41. Larkin, J. et al. Five-year survival with combined nivolumab and ipilimumab in advanced melanoma. *N. Engl. J. Med.* **381**, 1535–1546 (2019).
42. Schnell, A. et al. Stem-like intestinal Th17 cells give rise to pathogenic effector T cells during autoimmunity. *Cell* **184**, 6281–6298.e23 (2021).
43. Hirota, K. et al. Fate mapping of IL-17-producing T cells in inflammatory responses. *Nat. Immunol.* **12**, 255–263 (2011).
44. Nistala, K. et al. Th17 plasticity in human autoimmune arthritis is driven by the inflammatory environment. *Proc. Natl Acad. Sci. USA* **107**, 14751–14756 (2010).
45. Paroni, M. et al. Recognition of viral and self-antigens by  $T_H1$  and  $T_H1/T_{H17}$  central memory cells in patients with multiple sclerosis reveals distinct roles in immune surveillance and relapses. *J. Allergy Clin. Immunol.* **140**, 797–808 (2017).
46. Bamias, G. et al. Immunological characteristics of colitis associated with anti-CTLA-4 antibody therapy. *Cancer Invest.* **35**, 443–455 (2017).
47. Callahan, M. K. et al. Evaluation of serum IL-17 levels during ipilimumab therapy: correlation with colitis. *J. Clin. Oncol.* **29**, 2505–2505 (2011).
48. Reschke, R. et al. Checkpoint blockade-induced dermatitis and colitis are dominated by tissue-resident memory T cells and Th1/Tc1 cytokines. *Cancer Immunol. Res.* **10**, 1167–1174 (2022).
49. Dulos, J. et al. PD-1 blockade augments Th1 and Th17 and suppresses Th2 responses in peripheral blood from patients with prostate and advanced melanoma cancer. *J. Immunother.* **35**, 169–178 (2012).
50. Papotto, P. H., Ribot, J. C. & Silva-Santos, B. IL-17<sup>+</sup> γδ T cells as kick-starters of inflammation. *Nat. Immunol.* **18**, 604–611 (2017).
51. Huber, M. et al. A Th17-like developmental process leads to CD8<sup>+</sup> Tc17 cells with reduced cytotoxic activity. *Eur. J. Immunol.* **39**, 1716–1725 (2009).
52. Globig, A. M. et al. High-dimensional profiling reveals Tc17 cell enrichment in active Crohn's disease and identifies a potentially targetable signature. *Nat. Commun.* **13**, 3688 (2022).
53. Lim, S. Y. et al. Circulating cytokines predict immune-related toxicity in melanoma patients receiving anti-PD-1-based immunotherapy. *Clin. Cancer Res.* **25**, 1557–1563 (2019).
54. Luoma, A. M. et al. Molecular pathways of colon inflammation induced by cancer immunotherapy. *Cell* **182**, 655–671.e22 (2020).
55. Groom, J. R. & Luster, A. D. CXCR3 ligands: redundant, collaborative and antagonistic functions. *Immunol. Cell Biol.* **89**, 207–215 (2011).
56. Kisuya, J., Chemtai, A., Raballah, E., Keter, A. & Ouma, C. The diagnostic accuracy of Th1 (IFN-γ, TNF-α, and IL-2) and Th2 (IL-4, IL-6 and IL-10) cytokines response in AFB microscopy smear negative PTB- HIV co-infected patients. *Sci. Rep.* **9**, 2966 (2019).
57. Parameswaran, N. & Patial, S. Tumor necrosis factor-α signaling in macrophages. *Crit. Rev. Eukaryot. Gene Expr.* **20**, 87–103 (2010).
58. Varaljai, R. et al. Interleukin 17 signaling supports clinical benefit of dual CTLA-4 and PD-1 checkpoint inhibition in melanoma. *Nat. Cancer* **4**, 1292–1308 (2023).
59. Zhang, Y. et al. Interleukin-17-induced neutrophil extracellular traps mediate resistance to checkpoint blockade in pancreatic cancer. *J. Exp. Med.* **217**, e20190354 (2020).
60. Das, S. & Johnson, D. B. Immune-related adverse events and anti-tumor efficacy of immune checkpoint inhibitors. *J. Immunother. Cancer* **7**, 306 (2019).
61. Xing, P. et al. Incidence rates of immune-related adverse events and their correlation with response in advanced solid tumours treated with NIVO or NIVO+IPI: a systematic review and meta-analysis. *J. Immunother. Cancer* **7**, 341 (2019).
62. Nunez, N. G. et al. Immune signatures predict development of autoimmune toxicity in patients with cancer treated with immune checkpoint inhibitors. *Med* **4**, 113–129.e7 (2023).
63. Sterken, J. A. & Poschenrieder, A. J. Bioanalytical chemistry of cytokines—a review. *Anal. Chim. Acta* **853**, 95–115 (2015).
64. Chen, G. et al. Th17 cell frequency and IL-17A production in peripheral blood of patients with non-small-cell lung cancer. *J. Int. Med. Res.* **48**, 300060520925948 (2020).
65. Ozaki, K. & Leonard, W. J. Cytokine and cytokine receptor pleiotropy and redundancy. *J. Biol. Chem.* **277**, 29355–29358 (2002).
66. Gershenwald, J. E. et al. Melanoma staging: evidence-based changes in the American Joint Committee on Cancer eighth edition cancer staging manual. *CA Cancer J. Clin.* **67**, 472–492 (2017).
67. Eisenhauer, E. A. et al. New response evaluation criteria in solid tumours: revised RECIST guideline (version 1.1). *Eur. J. Cancer* **45**, 228–247 (2009).
68. Bolton, J. et al. Multiplex serological assay for establishing serological profiles of polymorphic, closely related peptide antigens. *MethodsX* **8**, 101345 (2021).
69. Assarsson, E. et al. Homogenous 96-plex PEA immunoassay exhibiting high sensitivity, specificity, and excellent scalability. *PLoS ONE* **9**, e95192 (2014).
70. Dries, R. et al. Giotto: a toolbox for integrative analysis and visualization of spatial expression data. *Genome Biol.* **22**, 78 (2021).
71. Germain, P. L., Lun, A., Garcia Meixide, C., Macnair, W. & Robinson, M. D. Doublet identification in single-cell sequencing data using scDblFinder. *F1000Res* **10**, 979 (2021).
72. Hao, Y. et al. Integrated analysis of multimodal single-cell data. *Cell* **184**, 3573–3587.e29 (2021).
73. Aran, D. et al. Reference-based analysis of lung single-cell sequencing reveals a transitional profibrotic macrophage. *Nat. Immunol.* **20**, 163–172 (2019).
74. Korsunsky, I. et al. Fast, sensitive and accurate integration of single-cell data with Harmony. *Nat. Methods* **16**, 1289–1296 (2019).

## Acknowledgements

F.D. is supported by the Swiss Academy of Medical Sciences (SAMS) and the Gottfried and Julia Bangerter-Rhyner Foundation (YTCR 22/19). P.F.C. is supported by the Fonds zur Förderung des akademischen Nachwuchses (FAN) University of Zurich Alumni fellowship. The Melanoma Biobank is supported by the University Research Priority Program in Translational Cancer Research (U-402-04-02) and the SKINTEGRITY.CH Consortium Biobank is supported by a grant from the Monique Doronville de la Cour Stiftung and the ETH Foundation. M.P.L. is supported by a grant from the Swiss National Science Foundation (CRSII5\_183478 / 1). We acknowledge the biobank team of the Dermatology Department of the University Hospital of Zurich and especially M. Schmid for her technical support and detailed work. We thank A. Ghosh and A. Cabral de Gouvea from the Functional Genomics Center Zurich, University of Zurich. We thank G. Restivo for providing us with the normal skin samples that were stained with multiplex immunofluorescence. We thank M. Tusup and S. Hogan for their important inputs in the study design. We thank all patients and families who participated in the study.

## Author contributions

F.D., M.P.L. and R.D. conceived the study. F.D., P.F.C., A.S., R.S., V.H., A.T., S.D., M.P.L., G.V.L. and B.B. designed the methodology. F.D., P.F.C., A.S., D.M.P., K.S.G., R.G., F.S. and C.U. performed the investigation. F.D. and P.F.C. were responsible for the quality control of data and algorithms. F.D., P.F.C. and A.S. analyzed and interpreted the data. P.F.C. conducted statistical analysis. F.D. acquired funding. F.D. wrote the manuscript.

F.D., P.F.C., A.S., A.T., K.S., R.G., V.H., G.V.L., B.B., M.P.L., C.M.M. and O.M. edited the manuscript. All authors revised the manuscript and approved the submission. All authors had full access to all the data and the final responsibility to submit for publication.

## Competing interests

This research received financial support from the Iten-Kohaut Stiftung Foundation and the University Hospital of Zurich (USZF27070) (F.D.), as well as from the Young Talents in Clinical Research program of the SAMS and Gottfried and Julia Bangerter-Rhyner Foundation (YTCR 01/22) (F.D.). F.D. receives or has received honoraria and travel support from Merck Sharp & Dohme, Bristol-Myers Squibb, Pierre Fabre and Sun Pharma outside the submitted work. K.S.G. receives research funding from Kyowa Kirin and Almirall. O.M. has a consulting advisory role for Bristol-Myers Squibb and Pierre Fabre, receives research funding from Bristol-Myers Squibb, Roche, Pierre Fabre, Amgen and MSD along with travel and accommodation expenses from Bristol-Myers Squibb. R.G. reports honoraria from Bristol-Myers Squibb, Merck Sharp & Dohme, Roche/Genentech, Novartis, Merck Serono, Almirall Hermal, Amgen, Sun Pharma, Pierre Fabre, Sanofi/Regeneron and Immunocore; a consulting or advisory role for Bristol-Myers Squibb, Merck Sharp & Dohme, Roche/Genentech, Novartis, Almirall Hermal, 4SC, Amgen, Pierre Fabre, Merck Serono, Sun Pharma, Sanofi, and Immunocore; research funding from Novartis, Amgen, Merck Serono, Sun Pharma, Sanofi, Almirall Hermal and Kyowa Kirin; and travel and accommodations expenses from Pierre Fabre, Sun Pharma and Boehringer Ingelheim. C.M.M. has received research grants to the institution from Eli Lilly, AstraZeneca, Roche, Amgen, Novartis, Novo Nordisk and MSD, including speaker or consultant fees. G.V.L. is consultant advisor for Agenus, Amgen, Array Biopharma, AstraZeneca, Boehringer Ingelheim, Bristol-Myers Squibb, Evaxion, Hexal AG (Sandoz Company), Highlight Therapeutics, Innovent Biologics USA, Merck Sharpe & Dohme, Novartis, OncoSec, PHMR, Pierre Fabre, Provectus, Qbiotics and Regeneron. M.P.L. has received project-specific research funding from Roche, Novartis, Molecular Partners and Oncobit. R.D. has intermittent, project-focused consulting and/or advisory relationships with Novartis, Merck Sharp & Dohme, Bristol-Myers Squibb, Roche, Amgen, Takeda, Pierre Fabre, Sun Pharma, Sanofi, Catalym, Second Genome, Regeneron, Alligator, T3 Pharma, MaxiVAX SA, Pfizer and

touchIME, all of which took place outside the submitted work. All other authors declare no competing interests.

## Additional information

**Extended data** is available for this paper at  
<https://doi.org/10.1038/s43018-024-00810-4>.

**Supplementary information** The online version contains supplementary material available at <https://doi.org/10.1038/s43018-024-00810-4>.

**Correspondence and requests for materials** should be addressed to Florentia Dimitriou or Reinhard Dummer.

**Peer review information** *Nature Cancer* thanks Genevieve Boland, Zlatko Trajanoski and the other, anonymous, reviewer(s) for their contribution to the peer review of this work.

**Reprints and permissions information** is available at [www.nature.com/reprints](http://www.nature.com/reprints).

**Publisher's note** Springer Nature remains neutral with regard to jurisdictional claims in published maps and institutional affiliations.

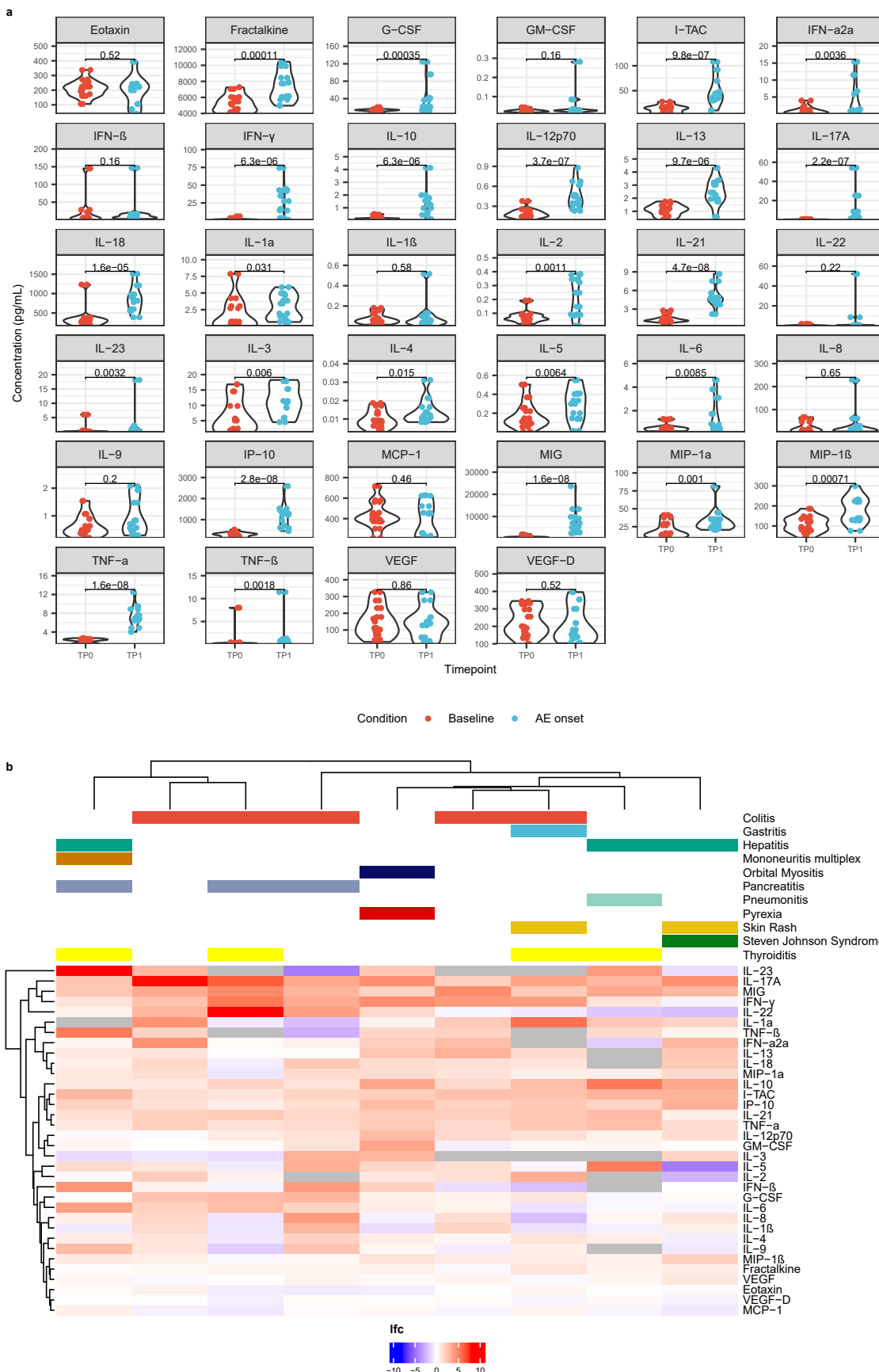
**Open Access** This article is licensed under a Creative Commons Attribution-NonCommercial-NoDerivatives 4.0 International License, which permits any non-commercial use, sharing, distribution and reproduction in any medium or format, as long as you give appropriate credit to the original author(s) and the source, provide a link to the Creative Commons licence, and indicate if you modified the licensed material. You do not have permission under this licence to share adapted material derived from this article or parts of it. The images or other third party material in this article are included in the article's Creative Commons licence, unless indicated otherwise in a credit line to the material. If material is not included in the article's Creative Commons licence and your intended use is not permitted by statutory regulation or exceeds the permitted use, you will need to obtain permission directly from the copyright holder. To view a copy of this licence, visit <http://creativecommons.org/licenses/by-nc-nd/4.0/>.

© The Author(s) 2024

<sup>1</sup>Department of Dermatology, University Hospital of Zurich, Zurich, Switzerland. <sup>2</sup>Faculty of Medicine, University of Zurich, Zurich, Switzerland.

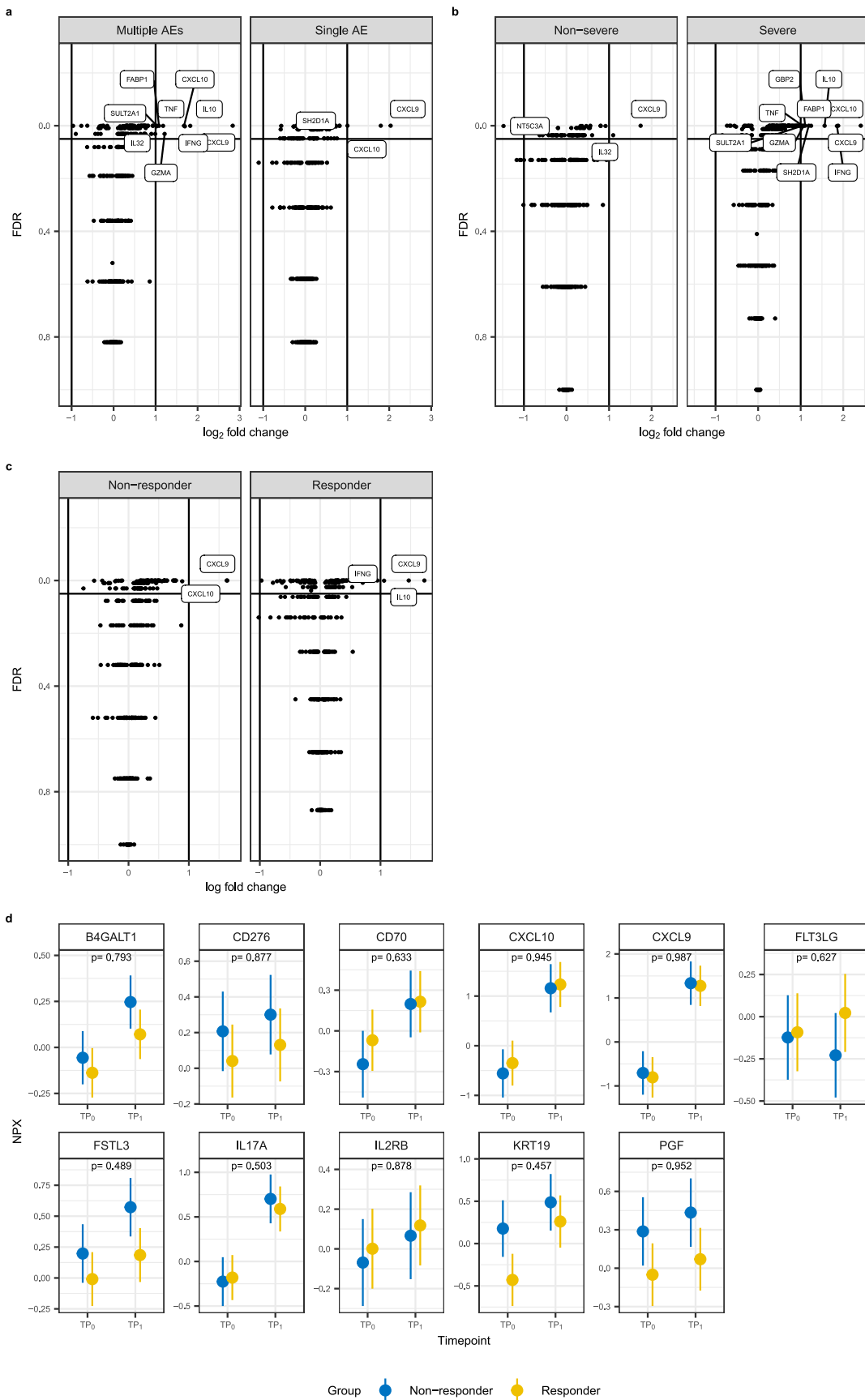
<sup>3</sup>Department of Oncology, Geneva University Hospital, Geneva, Switzerland. <sup>4</sup>Department of Dermatology, Johannes Wesling Medical Center, Ruhr University Bochum Campus Minden, Minden, Germany. <sup>5</sup>Department of Dermatology, Medical School Hannover, Hannover, Germany.

<sup>6</sup>Functional Genomics Center Zurich, University of Zurich/ETH Zurich, Zurich, Switzerland. <sup>7</sup>Institute for Pathology and Molecular Pathology, University Hospital Zurich, Zurich, Switzerland. <sup>8</sup>Department of Cardiology, University Heart Center and Center for Experimental Cardiology (CTEC), University Hospital Zurich and University of Zurich, Zurich, Switzerland. <sup>9</sup>Melanoma Institute Australia, The University of Sydney, Sydney, New South Wales, Australia. <sup>10</sup>Department of Medical Oncology, Royal North Shore and Mater Hospitals, Sydney, New South Wales, Australia. <sup>11</sup>Faculty of Medicine and Health, The University of Sydney, Sydney, New South Wales, Australia. <sup>12</sup>Institute of Experimental Immunology, University of Zurich (UZH), Zurich, Switzerland. <sup>13</sup>These authors contributed equally: Mitchell P. Levesque, Reinhard Dummer. ✉e-mail: [florentia.dimitriou@usz.ch](mailto:florentia.dimitriou@usz.ch); [Reinhard.Dummer@usz.ch](mailto:Reinhard.Dummer@usz.ch)



**Extended Data Fig. 1 | Discovery cohort.** Concentrations (pg/ml) of cytokines and chemokines from baseline to the grade  $\geq 3$  immune-related adverse event (AE) onset in the discovery cohort. Boxplot with each protein by timepoint of  $n = 9$  biological replicates for each timepoint (TP0 and TP1). Timepoint medians

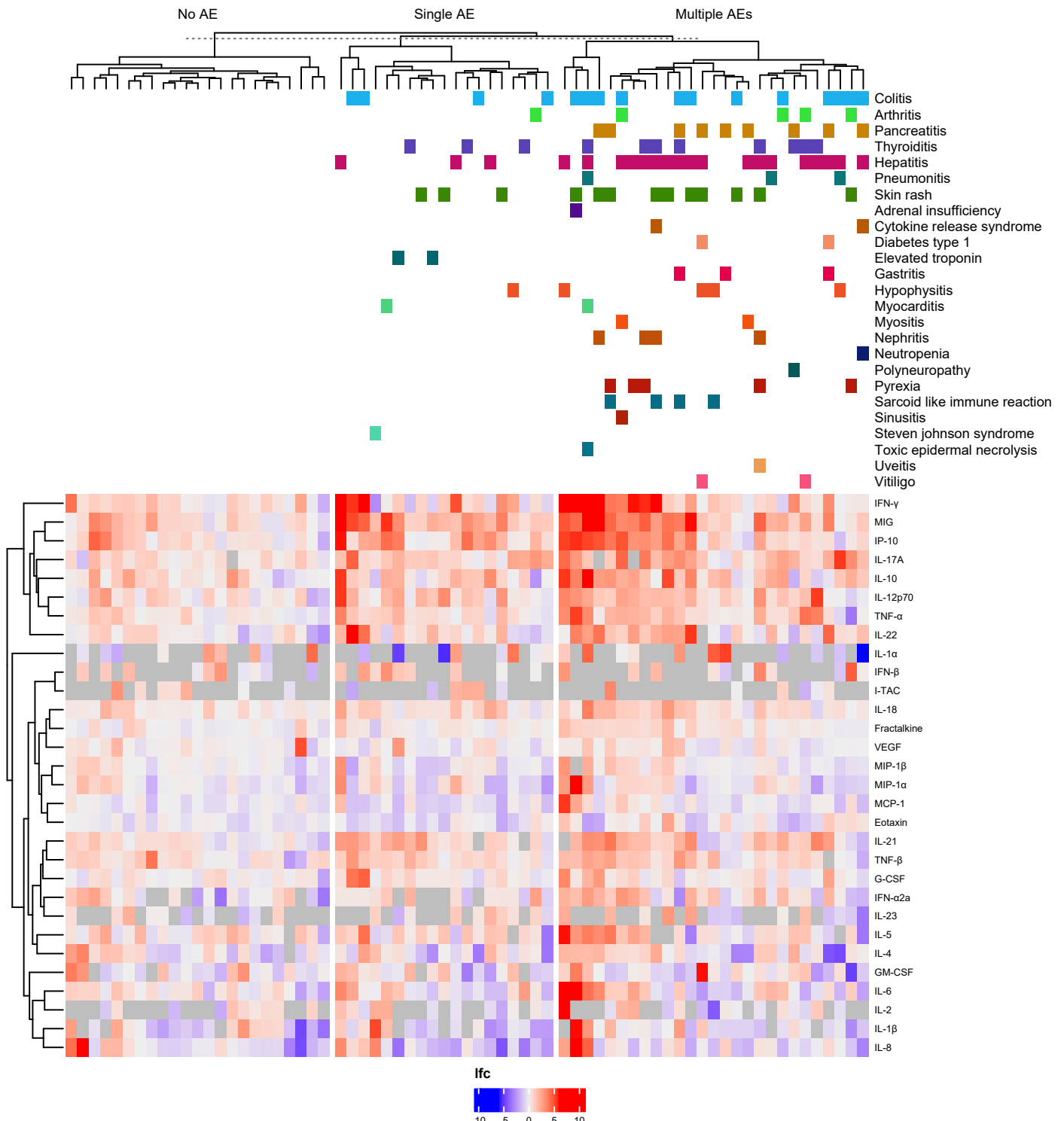
were compared using a two-sided Wilcoxon rank sum test and  $p$  values adjusted by the Benjamini-Hochberg method (a). Heatmap of  $\log_2$  fold change of serum cytokines and chemokines from baseline to grade  $\geq 3$  irAE onset for each patient ( $n = 9$ ) (b).



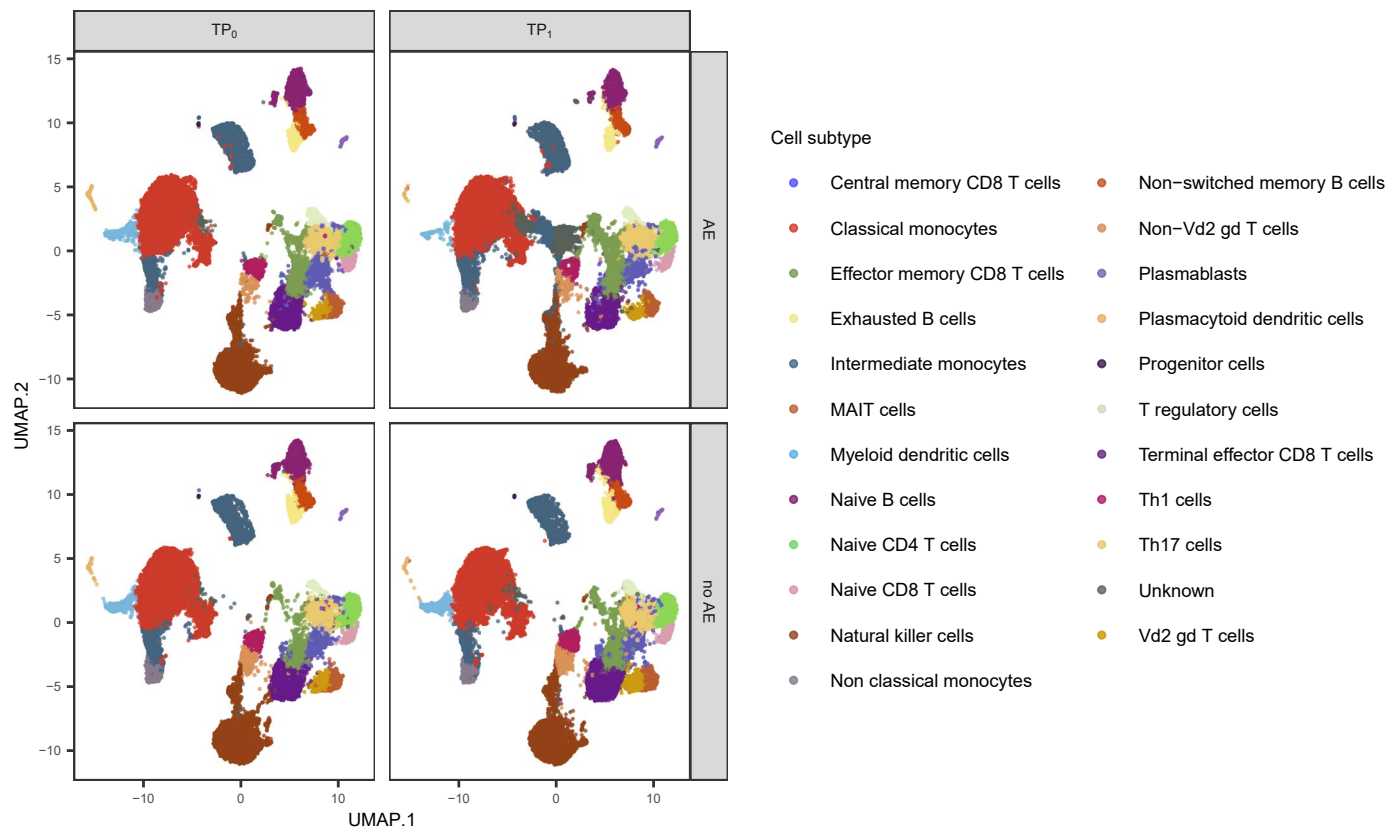
Extended Data Fig. 2 | See next page for caption.

**Extended Data Fig. 2 | Differential protein analysis by Olink in patient subgroups in the main study cohort.** Volcano plot with the differential expressed proteins at baseline (TPO) and at the AE onset (in patients with AEs) or at the second to fifth infusion (in patients without AEs) (TP1) in patients with multiple and single AEs (a), severe and non-severe AEs (b) and according to treatment response in the main study cohort ( $n = 73$ ) (c). Significant difference was determined by two-sided Wilcoxon rank sum test and  $p$ -values were adjusted

by the Benjamini-Hochberg method. Linear mixed effects regression analysis of the 11 significant proteins for the two time points (TPO and TP1) according to treatment response, in  $n = 36$  responders and  $n = 37$  non-responders. Data represented by estimated marginal means with 95% confidence intervals.  $P$ -values are adjusted using the tukey method (d). The y axis represents the Olink assay value (NPX).

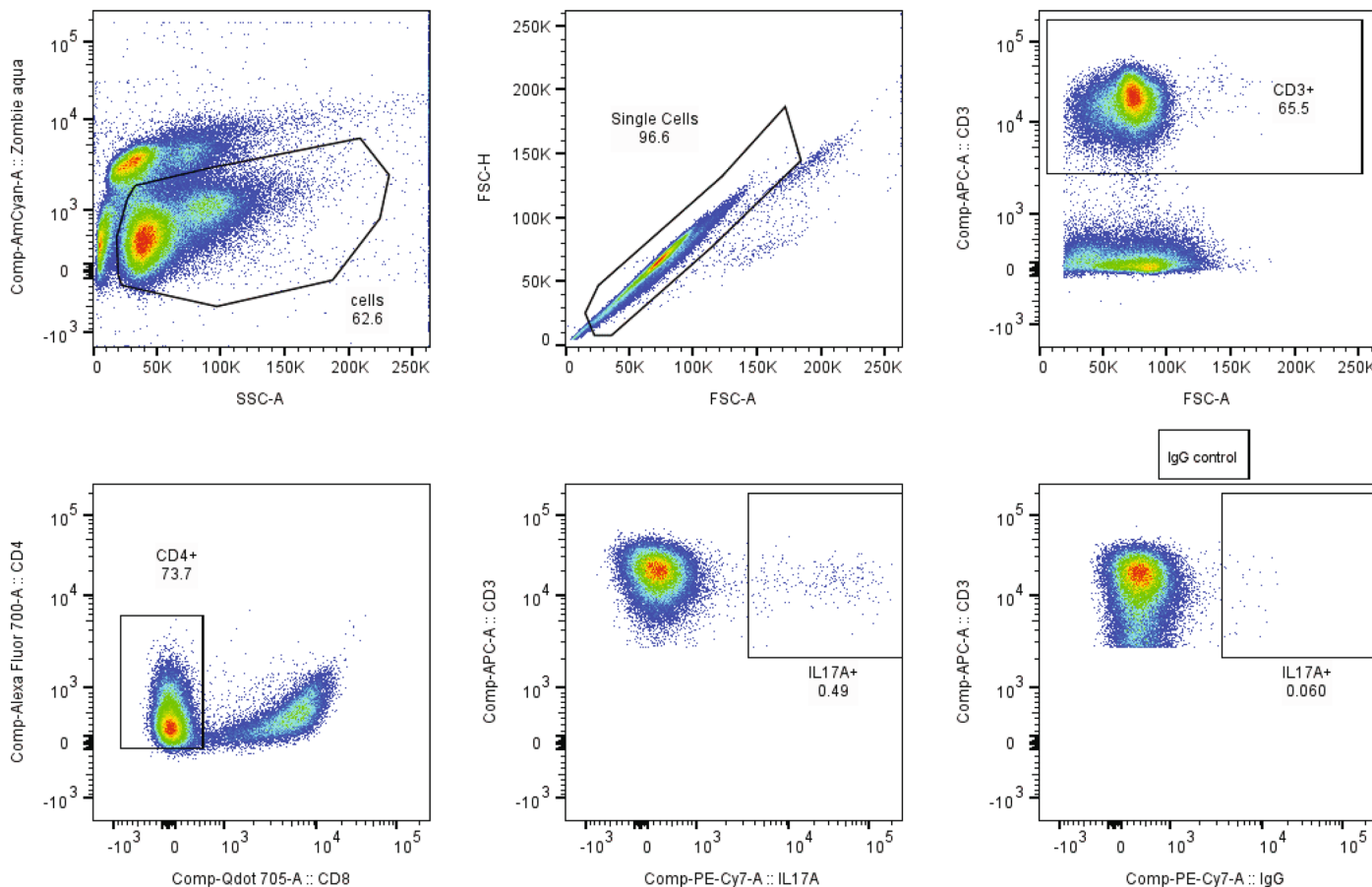


**Extended Data Fig. 3 | Overview of the multiplex chemokine/cytokine assay analysis in the main study cohort.** Heatmap of log<sub>2</sub> fold change of the serum cytokines and chemokines per patient in the multiplex MSD assay, split by type of AE (none, single AE and multiple AEs) in the main study cohort (n = 73).



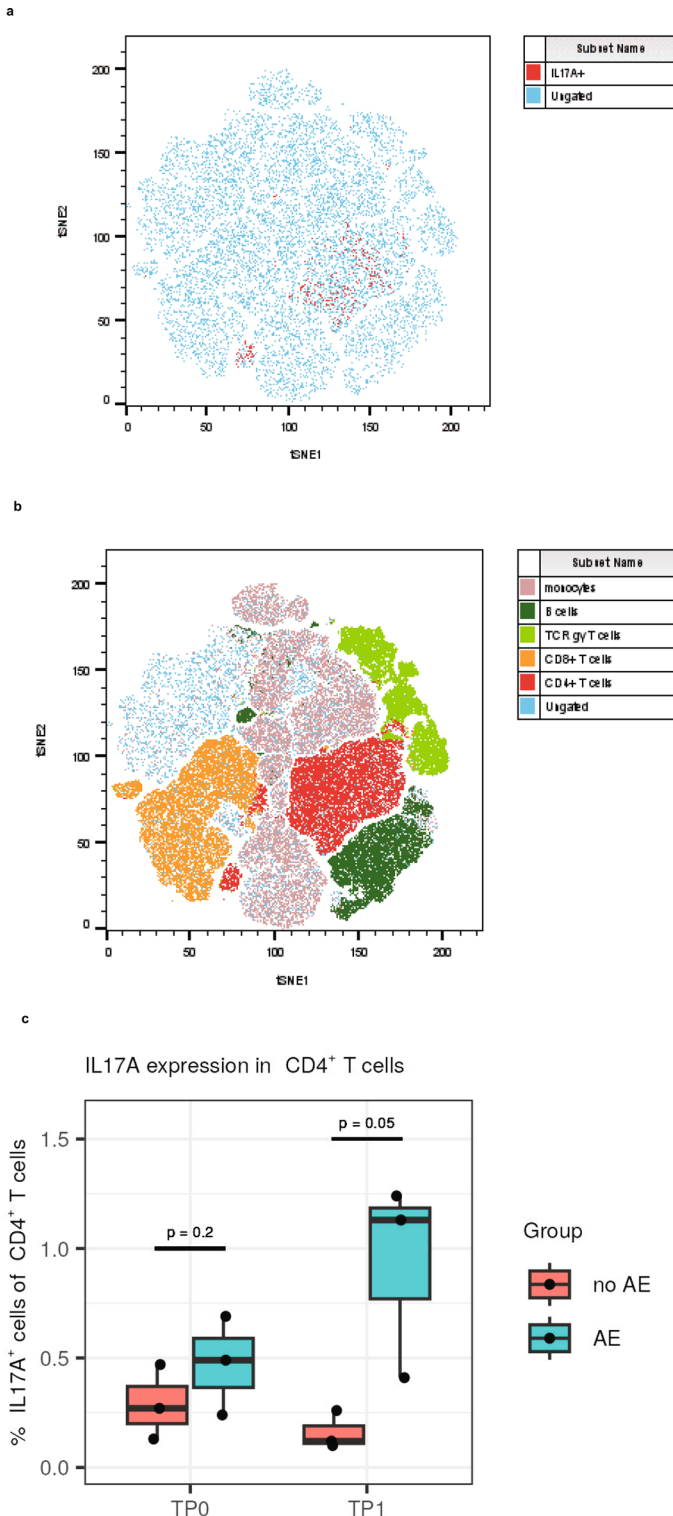
**Extended Data Fig. 4 | Uniform Manifold Approximation and Projection (UMAP) with overview of the main immune cell types split by time point and condition.** Single cell RNA sequencing analysis from the peripheral blood

mononuclear cells (PBMCs) samples at the baseline and at the irAEs onset from three patients with AEs and at the baseline and second to fifth infusion in three patients without any AEs.



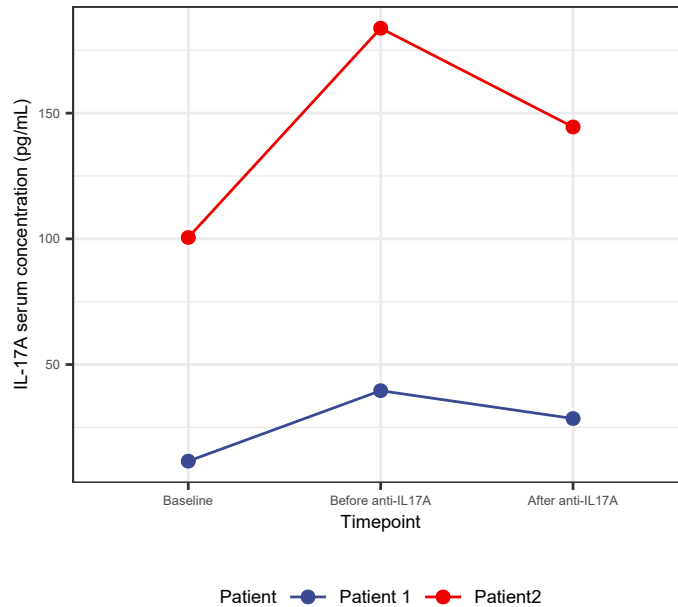
**Extended Data Fig. 5 | Flow cytometry (FC) gating strategy.** FC was used to determine IL-17A expression. Live cells were identified based on viability dye and SSC-A, and doublets were excluded based on FSC-H vs. FSC-A. T cells

were identified based on expression of CD3, and CD4 + T cells were defined as CD4 + CD8-. For gating of IL17A+ cells, the threshold was set based on an IgG control staining and applied uniformly to all samples in the dataset.



**Extended Data Fig. 6 | Flow cytometry (FC) analysis from the collected PBMCs in six patients with (n = 3) and without (n = 3) irAEs.** Uniform Manifold Approximation and Projection (UMAP) with overview of the main identified cell types; the FC analysis included antibodies targeting CD4+ and CD8+ T-cells, NK cells, B cells, monocytes, dendritic cells and  $\gamma\delta$  T-cells were included (a). UMAP

for IL-17A-producing cells (b). Proportional analysis of the IL-17A-producing CD4+ T-cells for the two time points (TP0 and TP1) in six patients with (n = 3) and without (n = 3) irAEs. Significant difference was determined by two-sided Wilcoxon rank sum test (c).



**Extended Data Fig. 7 | IL-17A serum concentration levels at the baseline (T0), before and after the administration of anti-IL17A in the two patients that were treated with secukinumab.** Secukinumab treatment was administered subcutaneously at a dose of 300 mg weekly for weeks 0 to 4, followed by 300 mg every 4 weeks.

## Reporting Summary

Nature Portfolio wishes to improve the reproducibility of the work that we publish. This form provides structure for consistency and transparency in reporting. For further information on Nature Portfolio policies, see our [Editorial Policies](#) and the [Editorial Policy Checklist](#).

### Statistics

For all statistical analyses, confirm that the following items are present in the figure legend, table legend, main text, or Methods section.

n/a Confirmed

- The exact sample size ( $n$ ) for each experimental group/condition, given as a discrete number and unit of measurement
- A statement on whether measurements were taken from distinct samples or whether the same sample was measured repeatedly
- The statistical test(s) used AND whether they are one- or two-sided  
*Only common tests should be described solely by name; describe more complex techniques in the Methods section.*
- A description of all covariates tested
- A description of any assumptions or corrections, such as tests of normality and adjustment for multiple comparisons
- A full description of the statistical parameters including central tendency (e.g. means) or other basic estimates (e.g. regression coefficient) AND variation (e.g. standard deviation) or associated estimates of uncertainty (e.g. confidence intervals)
- For null hypothesis testing, the test statistic (e.g.  $F$ ,  $t$ ,  $r$ ) with confidence intervals, effect sizes, degrees of freedom and  $P$  value noted  
*Give  $P$  values as exact values whenever suitable.*
- For Bayesian analysis, information on the choice of priors and Markov chain Monte Carlo settings
- For hierarchical and complex designs, identification of the appropriate level for tests and full reporting of outcomes
- Estimates of effect sizes (e.g. Cohen's  $d$ , Pearson's  $r$ ), indicating how they were calculated

*Our web collection on [statistics for biologists](#) contains articles on many of the points above.*

### Software and code

Policy information about [availability of computer code](#)

## Data collection

Clinical data was manually collected from patients' electronic records by a physician (FD). For the multiplex cytokine/chemokine assay, data was collected by the Discovery Workbench 4.0 (Mesoscale). Data collection for the proteomics was performed by Olink. For the single cell RNA sequencing, data was collected by Cellranger 7.0.0. For the flow cytometry, samples data was collected with the LSRFortessa™ Cell Analyzer (BD Biosciences). For the multiplex immunofluorescence, data was collected with the InForm 2.6.0 (Akoya Biosciences). For the spatial transcriptomics, data was collected using SpaceRanger 2.0.0.

## Data analysis

Clinical data was analyzed using gtsummary version 1.7.2. For the analysis of the multiplex cytokine/chemokine assay, Mesoscale electrochemiluminescence data was imported into the Mesoscale Discovery Workbench 4.0 analysis software for quantification. Quantified serum proteins were then imported into R version 4.3.0 for statistical analysis. For the analysis of the proteomic data, Olink proteomic data was imported with the OlinkAnalyze R package version 3.7.0. Single cells were filtered with the following parameters; >500 genes and <9000 genes detected, <40% mitochondrial RNA and defined as "singlet" by scDblFinder version 1.18.0 77. The Seurat v4 pipeline using SCTransform was used to normalize gene expression data. Cell typing was performed with SingleR (version 1.4.1) using the Monaco Immune dataset (GSE107011, PMID: 30726743). Differential expression was performed wmulith the FindMarkers function from the Seurat v4 package. ggplot2 version 3.5.0 was used for visualizing aggregated data. For the multiplex immunofluorescence, in-depth spatial expression analysis was performed using Giotto (version 2.0.0.957). Spatial transcriptomics data was analyzed with Seurat v4.0. Code to generate the figures is available at the github repository: pcheng84/AE\_analysis: Script to make figures for PBMC analysis (github.com)

For manuscripts utilizing custom algorithms or software that are central to the research but not yet described in published literature, software must be made available to editors and reviewers. We strongly encourage code deposition in a community repository (e.g. GitHub). See the Nature Portfolio [guidelines for submitting code & software](#) for further information.

## Data

Policy information about [availability of data](#)

All manuscripts must include a [data availability statement](#). This statement should provide the following information, where applicable:

- Accession codes, unique identifiers, or web links for publicly available datasets
- A description of any restrictions on data availability
- For clinical datasets or third party data, please ensure that the statement adheres to our [policy](#)

The data supporting the findings of this study are available within the manuscript. Single cell RNA sequencing and Visium aligned 10X single cell files that support the findings of this study are available at this link: <https://doi.org/10.5281/zenodo.10390377>. Source data for Figures 2, 3 and 5, as well as Extended Data Figures 1, 2, 3, 6 and 7 have been provided as Source Data files. All other relevant de-identified raw data related to the current study are available from the corresponding authors (Florentia.Dimitriou@usz.ch and Reinhard.Dummer@usz.ch) upon reasonable academic request and will require the researcher to sign a data access agreement with the University Hospital of Zurich. Individual patient identifiable data are not available due to concerns with patient identification.

## Research involving human participants, their data, or biological material

Policy information about studies with [human participants or human data](#). See also policy information about [sex, gender \(identity/presentation\), and sexual orientation](#) and [race, ethnicity and racism](#).

### Reporting on sex and gender

**Participant information on gender and age was self-reported. Information on gender, race and socioeconomic status was not collected. Patient information including gender and age are reported in Extended Data Table 1. Consent has been obtained for reporting and sharing individual-level data.**

### Reporting on race, ethnicity, or other socially relevant groupings

Race and ethnicity are not reported in the patient characteristics.

### Population characteristics

We included patients with advanced, stage III-IV (AJCCv8) melanoma treated with anti-PD1-based treatment in the Department of Dermatology at the University Hospital of Zurich. Patients received either nivolumab (240 mg every 2 weeks), pembrolizumab (200 mg every 3 weeks), or combination of nivolumab and ipilimumab (1 mg/kg nivolumab and 3 mg/kg ipilimumab every 3 weeks, followed by nivolumab monotherapy 240 mg every 2 weeks). Patients were treated in the metastatic setting. Previous treatments were allowed; however, irAEs from previous treatments had to be completely resolved or be ≤ grade 1 at the time of the treatment initiation for the inclusion in the study. Overall, previous ongoing irAEs were noted in four (5%) patients of the main study cohort and included immunotherapy-induced hypothyroidism due to previous immune-related thyroiditis in two patients, immune-related uveitis in one patient and immune-related hepatitis in one patient, with flare of the immune-related hepatitis upon ICI re-challenge. Patient demographics and clinicopathologic features were collected for all patients included in the study and are reported in Extended Data Table 1. These included sex, age, disease stage (AJCCv8), baseline LDH, previous treatments, as well as presence of autoimmune disease and ongoing toxicities from previous treatments at the treatment initiation. Treatment characteristics, including investigator-assessed treatment response, was assessed radiologically at regular time intervals and according to the RECIST 1.1 criteria.

### Recruitment

The discovery cohort was chosen from a retrospective cohort of 53 patients treated between January 2017 and August 2020, with available blood samples at the baseline and at the onset of the irAE. For the final analysis of the discovery cohort, nine patients with severe (≥ grade 3, CTCAEv5) irAEs that occurred early during the treatment and with available blood samples at baseline (0–29 days prior to therapy initiation) and at the irAEs onset were chosen. The discovery cohort was used as an exploratory cohort for the correlation of specific cytokines and chemokines with the irAEs onset.

The main study cohort was derived after establishment of a study protocol with a prospective sample collection in patients treated with anti-PD1-based ICIs, including both single-agent anti-PD1 (pembrolizumab and nivolumab) and anti-PD1 in combination with anti-CTLA4 (ipilimumab). In this prospective study cohort, blood samples were prospectively collected at baseline (0–29 days prior to therapy initiation) and at regular intervals during therapy from August 2019 to March 2021. For the final analysis of the prospective study cohort, blood samples at baseline (0–29 days prior to therapy initiation) and at the irAEs onset or at the second to fifth infusion (in patients without any irAEs) were chosen.

An independent external validation cohort of patients with advanced, stage III-IV (AJCCv8) melanoma treated from October 2019 until February 2022 with anti-PD1-based treatment in the Department of Dermatology at Medical School Hannover was used to validate these results. Blood samples at baseline and at the irAEs onset or at the second to fifth infusion (in patients without any irAEs) were chosen.

Potential biases applicable to this observational study are selection bias and immortal time bias, which were minimized by the definition of patient eligibility, the period of recruitment and the report of the follow-up period. The impact of these biases was further minimized by the validation of the study results with different methods (such as Mesoscale and Olink, single cell RNA sequencing and flow cytometry), as well as with an external validation cohort.

### Ethics oversight

Informed consent had been obtained from all patients and healthy tissue donors, as well as all study analyses conformed to the principles set out in the WMA Declaration of Helsinki and the Department of Health and Human Services Belmont Report. Skin from healthy, consenting individuals was obtained from adult abdominal healthy skin and was provided by the plastic surgery department of the University Hospital of Zurich with the assistance of SKINTEGRITY.CH biobank. Peripheral blood mononuclear cells and serum from patients were collected by the URPP cancer biobank. The use of material for research purposes was approved by the Zürich Cantonal Ethic Commission (KEK-Nr. 2020-01148 and KEK-Nr 2017-00688) and the ethics committee of Hannover Medical School (8685-2019). The study was conducted in accordance with the Declaration of Helsinki guidelines.

Anti-IL17A treatment was approved and reimbursed by the Federal Office of Public Health through a specific allowance in the Swiss health codes (article 71a KVV, from 27 June 1995). More information about Article 71a can be found on the website of the Swiss Department of Health: <https://www.bag.admin.ch/bag/en/home/versicherungen/krankenversicherung/krankenversicherung-leistungen-tarife/Arzneimittel/verguetung-artzneimittel-im-einzelfall.html>

Note that full information on the approval of the study protocol must also be provided in the manuscript.

## Field-specific reporting

Please select the one below that is the best fit for your research. If you are not sure, read the appropriate sections before making your selection.

- Life sciences       Behavioural & social sciences       Ecological, evolutionary & environmental sciences

For a reference copy of the document with all sections, see [nature.com/documents/nr-reporting-summary-flat.pdf](https://nature.com/documents/nr-reporting-summary-flat.pdf)

## Life sciences study design

All studies must disclose on these points even when the disclosure is negative.

Sample size	No statistical methods were used to pre-determine sample sizes, but our sample sizes are similar to those reported in previous publications (Lim, S.Y., et al. Circulating Cytokines Predict Immune-Related Toxicity in Melanoma Patients Receiving Anti-PD-1-Based Immunotherapy. <i>Clin Cancer Res</i> 25, 1557-1563 (2019)).
Data exclusions	Patients that did not meet the eligibility criteria were not included in the study. No data were excluded from the analyses.
Replication	Experiments involving Olink proteomic data, single cell RNA sequencing, multiplex immunofluorescence and spatial transcriptomics were performed once. For the multiplex cytokine/chemokine assay (Mesoscale Diagnostics, Maryland), each run was performed in duplicate for the discovery cohort; duplicates did not vary by more than 4%. The flow cytometry experiment was performed in three replicates. All techniques and reagents used for the analyses of this study were previously optimized and validated.
Randomization	This is an observational study and data collection was not randomized.
Blinding	The Investigators were not blinded to allocation during experiments and outcome assessment. Data collection and analysis were not performed blind to the conditions of the experiments.

## Reporting for specific materials, systems and methods

We require information from authors about some types of materials, experimental systems and methods used in many studies. Here, indicate whether each material, system or method listed is relevant to your study. If you are not sure if a list item applies to your research, read the appropriate section before selecting a response.

Materials & experimental systems		Methods	
n/a	Involved in the study	n/a	Involved in the study
<input type="checkbox"/>	<input checked="" type="checkbox"/> Antibodies	<input checked="" type="checkbox"/>	<input type="checkbox"/> ChIP-seq
<input checked="" type="checkbox"/>	<input type="checkbox"/> Eukaryotic cell lines	<input type="checkbox"/>	<input checked="" type="checkbox"/> Flow cytometry
<input checked="" type="checkbox"/>	<input type="checkbox"/> Palaeontology and archaeology	<input checked="" type="checkbox"/>	<input type="checkbox"/> MRI-based neuroimaging
<input checked="" type="checkbox"/>	<input type="checkbox"/> Animals and other organisms		
<input checked="" type="checkbox"/>	<input type="checkbox"/> Clinical data		
<input checked="" type="checkbox"/>	<input type="checkbox"/> Dual use research of concern		
<input checked="" type="checkbox"/>	<input type="checkbox"/> Plants		

## Antibodies

Antibodies used	Multiplex immunofluorescence: panCK sc-8016 (Santa Cruz, dilution 1:100), CD4 ab133616 (abcam, dilution 1:100), CD8 ab4055 (abcam, dilution 1:100), IL-17A ab79056 (abcam, dilution 1:100), FoxP3 14-4777-82 (Invitrogen), CD68 ab213363 (abcam)
	Flow cytometry: anti-human CD4 Antibody Cat #344621 (Biolegend, dilution 1:50), anti-human CD19 Antibody Cat #302205 (Biolegend, dilution 1:20), anti-human TCR γ/δ Antibody Cat #331209 (Biolegend, dilution 1:20), anti-human IL-17A Antibody Cat #512315 (Biolegend, dilution 1:20), anti-human HLA-DR Antibody Cat #307623 (Biolegend, dilution 1:50), anti-human CD8 Antibody Cat #344733 (Biolegend, dilution 1:100), Zombie Aqua Cat #423101(Biolegend, Zombie Aqua was reconstituted according to the manufacturer's instructions and diluted 1:1000 in PBS.), anti-human CD3 Antibody Cat #317318 (Biolegend, dilution 1:50), Cyto-Fast Fix/Perm Buffer Set Cat #426803 (Biolegend, Cyto-Fast Fix/Perm Buffer was used according to the manufacturer's instructions at 100 ul/sample. Cells were washed with 1x Cyto-Fast Perm Wash solution.), Mouse IgG1, κ Isotype Ctrl Antibody PE/Cy7 Cat #400125 (Biolegend, dilution 1:80)
Validation	Pan-Cytokeratin Antibody (C11) is a mouse monoclonal IgG1 κ pan-Cytokeratin antibody, cited in 150 publications and is raised against keratin-enriched human epidermoid carcinoma cell line A-431. CD4, CD8, CD68, IL-17A abcam antibodies and FocP3

Invitrogen antibodies have been validated by the manufacturer for IHC-P and/or ICC/IF. All Biolegend antibodies have been quality tested for flow cytometry by the manufacturer. An FC quality statement can be found on the manufacturer's website: <https://www.biologend.com/>

## Plants

### Seed stocks

Report on the source of all seed stocks or other plant material used. If applicable, state the seed stock centre and catalogue number. If plant specimens were collected from the field, describe the collection location, date and sampling procedures.

### Novel plant genotypes

Describe the methods by which all novel plant genotypes were produced. This includes those generated by transgenic approaches, gene editing, chemical/radiation-based mutagenesis and hybridization. For transgenic lines, describe the transformation method, the number of independent lines analyzed and the generation upon which experiments were performed. For gene-edited lines, describe the editor used, the endogenous sequence targeted for editing, the targeting guide RNA sequence (if applicable) and how the editor was applied.

### Authentication

Describe any authentication procedures for each seed stock used or novel genotype generated. Describe any experiments used to assess the effect of a mutation and, where applicable, how potential secondary effects (e.g. second site T-DNA insertions, mosaicism, off-target gene editing) were examined.

## Flow Cytometry

### Plots

Confirm that:

- The axis labels state the marker and fluorochrome used (e.g. CD4-FITC).
- The axis scales are clearly visible. Include numbers along axes only for bottom left plot of group (a 'group' is an analysis of identical markers).
- All plots are contour plots with outliers or pseudocolor plots.
- A numerical value for number of cells or percentage (with statistics) is provided.

### Methodology

#### Sample preparation

Sample preparation is described in the Methods section of the manuscript: Cell stimulation and intracellular cytokine staining for flow cytometry

#### Instrument

LSRFortessa™ Cell Analyzer (BD Biosciences)

#### Software

FlowJo v10.8.1

#### Cell population abundance

A total of 482 IL17A+ cells were identified across all samples

#### Gating strategy

Cells were gated as live cells using flexible viability dye (zombie aqua) and SSC-A, then as single cells using FSC-H and FSC-A. Single cells from all samples were concatenated to create tSNE maps. As IL17A+ cells were only detected amongst CD3+ CD4+ cells, each samples were then again gated individually for CD3+ cells, then as CD4+CD8- cells. From these cells, the gate for IL17A was adjusted on the sample with the highest abundance of IL17A+ cells (according to the tSNE map), and the gate was adjusted comparing to the IgG control of the same sample. This gate was then transferred to all other samples without adjustment.

Tick this box to confirm that a figure exemplifying the gating strategy is provided in the Supplementary Information.